



## Original Paper

# Accurate simulations of pure-viscoacoustic wave propagation in tilted transversely isotropic media

Qiang Mao <sup>a, b</sup>, Jian-Ping Huang <sup>a, b, \*</sup>, Xin-Ru Mu <sup>a, b</sup>, Ji-Dong Yang <sup>a, b</sup>, Yu-Jian Zhang <sup>a, b</sup>

<sup>a</sup> Geosciences Department, China University of Petroleum (East China), Qingdao, 266580, Shandong, China

<sup>b</sup> Pilot National Laboratory for Marine Science and Technology (Qingdao), Qingdao, 266207, Shandong, China

## ARTICLE INFO

## Article history:

Received 2 April 2023

Received in revised form

14 July 2023

Accepted 6 November 2023

Available online 10 November 2023

Edited by Jie Hao and Meng-Jiao Zhou

## Keywords:

Pure-viscoacoustic TTI wave equation

Attenuation anisotropy

Seismic modeling

Low-rank decomposition method

## ABSTRACT

Forward modeling of seismic wave propagation is crucial for the realization of reverse time migration (RTM) and full waveform inversion (FWI) in attenuating transversely isotropic media. To describe the attenuation and anisotropy properties of subsurface media, the pure-viscoacoustic anisotropic wave equations are established for wavefield simulations, because they can provide clear and stable wavefields. However, due to the use of several approximations in deriving the wave equation and the introduction of a fractional Laplacian approximation in solving the derived equation, the wavefields simulated by the previous pure-viscoacoustic tilted transversely isotropic (TTI) wave equations has low accuracy. To accurately simulate wavefields in media with velocity anisotropy and attenuation anisotropy, we first derive a new pure-viscoacoustic TTI wave equation from the exact complex-valued dispersion formula in viscoelastic vertical transversely isotropic (VTI) media. Then, we present the hybrid finite-difference and low-rank decomposition (HFDLRD) method to accurately solve our proposed pure-viscoacoustic TTI wave equation. Theoretical analysis and numerical examples suggest that our pure-viscoacoustic TTI wave equation has higher accuracy than previous pure-viscoacoustic TTI wave equations in describing qP-wave kinematic and attenuation characteristics. Additionally, the numerical experiment in a simple two-layer model shows that the HFDLRD technique outperforms the hybrid finite-difference and pseudo-spectral (HFDPs) method in terms of accuracy of wavefield modeling.

© 2024 The Authors. Publishing services by Elsevier B.V. on behalf of KeAi Communications Co. Ltd. This is an open access article under the CC BY-NC-ND license (<http://creativecommons.org/licenses/by-nc-nd/4.0/>).

## 1. Introduction

Field seismic data observations and laboratory rock sample measurements demonstrate that anisotropy and viscosity are widely distributed in the subsurface medium (Carcione, 1992; Thomsen, 1986; Best et al., 2007; Zhubayev et al., 2016). Velocity anisotropy is commonly associated in the subsurface medium with aligned structure (Thomsen, 1986; Alkhalifah, 2000). In addition, attenuation anisotropy will coexist with velocity anisotropy when seismic waves propagate through thin layers with various velocity and attenuation characteristics or aligned fluid-filled cracks (Liu et al., 2007; Carcione, 2010; Usher et al., 2017; Guo and McMechan, 2017). The amplitude dimming and waveform distortion of seismic waves are generated due to the viscosity and anisotropy properties of the real earth medium. If the

unsatisfactory effects of viscosity and anisotropy on seismic wave propagation are ignored during migration imaging, the location of the imaged interfaces will be deviated and the imaging resolution will be reduced (Dutta and Schuster, 2014; Qu et al., 2017). Therefore, it is important to precisely describe the effects of viscosity and anisotropy on seismic wave propagation in order to counteract these negative effects on high-precision imaging.

Viscosity, an anelastic property of the subsurface medium, which has been observed in many field surveys and laboratory measurements, particularly in the strong attenuation regions (e.g., hydrocarbon reservoir), will result in inherent attenuation effects (McDonal et al., 1958; Guo et al., 2016). The intrinsic attenuation characteristics can be expressed by the quality factor  $Q$  that quantifies the energy loss due to subsurface medium absorption at each wavelength (Aki and Richards, 1980; Zhu et al., 2013; Da Silva et al., 2019). In past decades, in order to simulate seismic wave propagation in viscoacoustic media, many viscoacoustic wave equations have been proposed based on the standard linear solid (SLS) model (Emmerich and Korn, 1987; Carcione et al., 1988;

\* Corresponding author.

E-mail address: [jphuang@upc.edu.cn](mailto:jphuang@upc.edu.cn) (J.-P. Huang).

Robertsson et al., 1994; Deng and McMechan, 2007; Zhu et al., 2013) and the constant  $Q$  model (Carcione et al., 2002; Carcione, 2010; Zhu and Harris, 2014; Wang et al., 2018, 2020). Viscoacoustic wave equations derived from constant  $Q$  theory (Kjartansson, 1979) have naturally separated amplitude dissipation terms and phase dispersion terms, which have attracted a lot of attention. Based on constant  $Q$  theory, a fractional Laplacian viscoacoustic wave equation proposed by Zhu and Harris (2014) is widely used for wavefield simulations and  $Q$ -compensated RTM in viscoacoustic media (Zhu et al., 2014; Sun et al., 2015; Li et al., 2016). Following that, several high-precision viscoacoustic wave equations have been developed recently (Mu et al., 2021; Yang and Zhu, 2018; Liu and Luo, 2021), which are based on constant  $Q$  theory.

Another widely existing characteristic of subsurface media is anisotropy. To describe anisotropy, four independent parameters are used by geophysicists to determine the phase and group velocities of seismic waves in the transversely isotropic (TI) medium (Tsvankin, 1996; Fomel, 2004; Li and Stovas, 2021). The propagation of seismic wave in anisotropic media can be precisely described by the multi-parameter dependent anisotropic elastic wave equations (Xu et al., 2020). However, these wave equations require a lot of computational resources in the application. Therefore, most studies have focused on deriving the wave equation in anisotropic media considering only P-waves (Zhang et al., 2011; Yan and Liu, 2016). Over the years, many acoustic anisotropic wave equations have been developed, which mainly fall under two categories: the coupled pseudo-acoustic anisotropic wave equations (Alkhalifah, 2000; Zhou et al., 2006; Du et al., 2007; Fletcher et al., 2009; Duveneck and Bakker, 2011; Zhang et al., 2011) and the pure-acoustic anisotropic wave equations (Chu et al., 2011; Zhan et al., 2012; Mu et al., 2020). Coupled pseudo-acoustic anisotropic wave equations can be efficiently applied to migration application and can well preserve the accurate kinematic characteristics of P-waves (Huang et al., 2023). Nevertheless, the coupled pseudo-acoustic anisotropic wave equation produces shear wave artifacts and is restricted by the anisotropy parameters range. Therefore, pure-acoustic anisotropic wave equations are developed to address the afore-mentioned issues. However, the pure-acoustic anisotropic wave equations have the disadvantage of requiring a large amount of computation time, and their kinematic accuracy is lower than that of the coupled pseudo-acoustic anisotropic wave equations, due to the approximations used in the derivation of the wave equations. As a result, one can choose from the different types of acoustic anisotropic wave equations based on their requirements.

Generally, attenuation and anisotropy characteristics of the subsurface media affect the seismic wavefield simultaneously during seismic wave propagation (Hao and Alkhalifah, 2019; Da Silva et al., 2019). To correct for the unsatisfactory effects of attenuation and anisotropy, some recent studies have focused on taking both attenuation and anisotropy into account in the derivation of the wave equation (Zhu et al., 2007; Carcione et al., 2012; Zhu and Bai, 2019). Based on an exact phase velocity formula and an SLS attenuation model, Xu et al. (2015) developed a pure-viscoacoustic TTI wave equation. Following that, several different types of the viscoacoustic anisotropic wave equations have been proposed recently, which can be used for wavefield simulations and  $Q$ -compensated RTM (Zhang et al., 2020a; Fathalian et al., 2021; Mu et al., 2022a). These viscoacoustic anisotropic wave equations, however, only take attenuation isotropy into account and do not account for attenuation anisotropy. Attenuation anisotropy has been shown to have a considerable influence on seismic wave propagation in some experimental and numerical studies (Carcione, 1992; Lynn et al., 1999; Chichinina et al., 2009; Behura and Tsvankin, 2009; Bai and Tsvankin, 2016; Zhubayev et al., 2016; Zhu, 2017; Hao and Alkhalifah, 2017). To better describe the

characteristics of seismic wave propagation in an attenuating anisotropic medium, Da Silva et al. (2019) derived a viscoacoustic TTI wave equation in the media with velocity anisotropy and attenuation anisotropy. In addition, by combining the acoustic anisotropic wave equation proposed by Duveneck et al. (2008) with constant  $Q$  attenuation theory, Qiao et al. (2020) derived a coupled pseudo-viscoacoustic TTI wave equation. Afterwards, Wang et al. (2022) derived a fractional Laplacian viscoelastic wave equation in attenuating anisotropic media, which can also be transformed into the coupled pseudo-viscoacoustic anisotropic wave equation under acoustic approximation. Unfortunately, these coupled pseudo-viscoacoustic anisotropic wave equations suffer from SV-wave artifacts. To address this issue, Mu et al. (2022b) and Qiao et al. (2022) independently developed the decoupled pure-viscoacoustic TTI wave equation in media with velocity and attenuation anisotropy. Nevertheless, in media with strong attenuation and anisotropy, the wavefields simulated by these pure-viscoacoustic TTI wave equations are inaccurate. As a result, it is necessary to develop a pure-viscoacoustic TTI wave equation with high accuracy for wavefield simulation in attenuating TTI media.

In addition, although the fractional Laplacian viscoacoustic anisotropic wave equations can be well used for wavefield simulations and  $Q$ -compensated RTM, the numerical simulation of the variable-order fractional Laplacian is an intractable problem. The average  $Q$  method proposed by Zhu and Harris (2014) is first used to address this issue. However, the fractional Laplacian solving by the average  $Q$  method is inaccurate in strongly heterogeneous attenuation media. To deal with this problem, several high-accuracy strategies have been proposed. Sun et al. (2015) proposed the one-step wave extrapolation method based on the low-rank decomposition (LROSE) to accurately solve the fractional Laplacian viscoacoustic wave equation. Later, the constant fractional order approximation method (Chen et al., 2016), the Hermite distributed approximating functional method (Yao et al., 2017), the matrix-transform numerical solver method (Chen et al., 2019b), and the high-order Taylor series expansion method (Zhang et al., 2020b) also were developed to solve the variable-order fractional Laplacian. Among the afore-mentioned methods, the low-rank decomposition approach has the advantage of higher accuracy in solving the fractional Laplacian (Chen et al., 2019a; Zhou et al., 2022; Zhang et al., 2023), which is of great significance for wavefield simulation in strongly attenuating media. However, the LROSE method derived by Sun et al. (2015) requires huge computational cost in complex viscoacoustic media. Therefore, in order to improve the computational speed of solving the viscoacoustic anisotropic wave equations, a combination of the low-rank decomposition method with the efficient finite-difference method is a satisfactory choice for solving viscoacoustic anisotropic wave equation with fractional Laplacian.

In this paper, starting from the exact complex-valued phase velocity formula in viscoelastic VTI media, we derive a new pure-viscoacoustic TTI wave equation using the new acoustic approximation that is totally S-wave free. Our new pure-viscoacoustic TTI wave equation can provide more accurate wavefield than the previous wave equations in media with velocity anisotropy and attenuation anisotropy. The accuracy of the proposed wave equation is first confirmed through the theoretical analysis. Then, with the help of the numerical tests, we further verify that the proposed wave equation has higher accuracy in describing qP-wave kinematic properties and attenuation characteristics than the pure-viscoacoustic TTI wave equation proposed by Mu et al. (2022b). In numerical simulations, we develop the hybrid finite-difference and low-rank decomposition (HFDLRD) method to accurately solve our new pure-viscoacoustic TTI wave equation. The numerical test in a simple two-layer shows that the proposed HFDLRD method

outperforms the hybrid finite-difference and pseudo-spectral (HFDPS) method in terms of accuracy.

This paper is organized as follows: First, we derive a new pure-viscoacoustic TTI wave equation through some mathematical manipulations. Theoretical analysis is used to verify the accuracy of our proposed wave equation. Then, we develop the HFDLRD method to calculate the newly derived wave equation. Finally, we perform numerical simulation in homogeneous and heterogeneous models to illustrate the accuracy and stability of the newly proposed wave equation, along with the accuracy of the HFDLRD method.

frequency-dependent complex-valued velocity can be used to describe the seismic wave propagation in attenuating media. By solving the viscoelastic Christoffel equation in VTI media, the exact complex-valued phase velocity formula in 2D viscoelastic media can be written as

$$V_p^2(\theta) = (M_{11} \sin^2 \theta + M_{33} \cos^2 \theta + M_{55} + E) / 2\rho, \quad (3)$$

$$V_{sv}^2(\theta) = (M_{11} \sin^2 \theta + M_{33} \cos^2 \theta + M_{55} - E) / 2\rho, \quad (4)$$

$$E = \sqrt{(M_{33} - M_{55}) \cos^2 \theta + (M_{55} - M_{11}) \sin^2 \theta)^2 + 4(M_{13} + M_{55})^2 \sin^2 \theta \cos^2 \theta}, \quad (5)$$

## 2. Methodology

### 2.1. Derivation of the new pure-viscoacoustic anisotropic equation

To simulate the linear attenuation in seismology and seismic exploration, the constant Q model proposed by Kjartansson (1979) is one of the widely used mathematical models. Based on constant Q theory, the frequency domain stress-strain relation in viscoelastic VTI media can be expressed as

$$\sigma_{ij}(\omega) = M_{ij}(\omega) \varepsilon_{ij}(\omega), \quad (1)$$

where  $\sigma_{ij}$  and  $\varepsilon_{ij}$  denote the stress and strain tensors, respectively. The complex stiffness coefficient  $M_{ij}(\omega)$  in Eq. (1) can be written as

$$M_{ij}(\omega) = C_{ij} \cos^2(\pi\gamma_{ij}/2) \left(\frac{i\omega}{\omega_0}\right)^{2\gamma_{ij}}, \quad (2)$$

where  $V_p(\theta)$  and  $V_{sv}(\theta)$  denote the P- and SV-wave phase velocity, respectively.  $\theta$  and  $\rho$  are the phase angle and the density, respectively.

Based on Eq. (3), using the acoustic approximation and other approximations, some pure-viscoacoustic TTI wave equations have been developed recently (Qiao et al., 2022; Mu et al., 2022b). Nevertheless, due to the use of these approximations in deriving the wave equation, the previous pure-viscoacoustic TTI wave equations have low simulation accuracy. Therefore, on the basis of the new acoustic approximation (Xu et al., 2020), we derive a high-precision pure-viscoacoustic TTI wave equation in this study. First, the complex stiffness coefficient  $M_{13}$  in Eq. (5) can be approximated using the expression given as follows (Qiao et al., 2019):

$$M_{13} \approx M_{33}(1 + \delta) - 2M_{55}. \quad (6)$$

Substituting Eq. (6) into Eq. (5), after several mathematical

$$E \approx \sqrt{(M_{33} \cos^2 \theta + M_{11} \sin^2 \theta - M_{55})^2 + 4[(1 + 2\delta)M_{33}^2 + (M_{11} - (1 + 2\delta)M_{33})M_{55} - M_{11}M_{33}] \sin^2 \theta \cos^2 \theta}. \quad (7)$$

where  $\omega$  denotes the angular frequency,  $\omega_0$  denotes the reference angular frequency,  $\gamma_{ij} = \arctan(1/Q_{ij})/\pi$  are dimensionless parameters related to the quality factor and the value of  $\gamma_{ij}$  in Eq. (2) is (0, 0.5) for any positive quality factor  $Q_{ij}$ . The elastic stiffness coefficient  $C_{ij}$  can be computed from Thomsen anisotropy parameters  $\varepsilon$  and  $\delta$  (Thomsen, 1986). The Q-related Thomsen anisotropy parameters  $\varepsilon_Q$  and  $\delta_Q$  can be used to characterize the anisotropic quality factors  $Q_{ij}$  (Zhu and Tsvankin, 2006). Additionally, the

manipulations, Eq. (5) can be expressed as

Drawing on the work of Xu et al. (2020), we make SV-wave phase velocity  $V_{sv}(\theta)$  to zero along all the direction, which yields

$$M_{11} \sin^2 \theta + M_{33} \cos^2 \theta + M_{55} = E. \quad (8)$$

Based on Eqs. (7) and (8), the expression of  $M_{55}$  can be given as

$$M_{55} = \frac{[(1 + 2\delta)M_{33}^2 - M_{11}M_{33}] \sin^2 \theta \cos^2 \theta}{[(M_{11} \sin^2 \theta + M_{33} \cos^2 \theta) - (M_{11} - (1 + 2\delta)M_{33}) \sin^2 \theta \cos^2 \theta]}. \quad (9)$$

By substituting Eqs. (8) and (9) into Eq. (3), and we assume that the density is constant and equals to 1, Eq. (3) can be written as

$$V_p^2(\theta) = M_{11} \sin^2 \theta + M_{33} \cos^2 \theta + \frac{[(1 + 2\delta)M_{33}^2 - M_{11}M_{33}] \sin^2 \theta \cos^2 \theta}{[(M_{11} \sin^2 \theta + M_{33} \cos^2 \theta) - (M_{11} - (1 + 2\delta)M_{33}) \sin^2 \theta \cos^2 \theta]} \quad (10)$$

Eq. (10) is a pure P-wave phase velocity formula. In addition, we can observe that Eq. (10) only contains one anisotropy attenuation parameter due to the approximation (Eq. (6)) we adopted. To address this issue, we make an assumption that  $\sqrt{1 + 2\delta}M_{33} \approx M_{13}$ , because for  $\delta \in (-0.2, 0.4)$ ,  $\delta_Q \in (-1.2, 0.6)$  and  $Q_p \geq 10$ , there is  $|(M_{13} - \sqrt{1 + 2\delta}M_{33})/M_{13}| \leq 0.0995$ , noting that  $M_{13} = \sqrt{1 + 2\delta}C_{33} \cos^2(\pi\gamma_{13}/2)(i\omega/\omega_0)^{2\gamma_{13}}$  and the expression  $\gamma_{13}$  is defined as  $\gamma_{13} = \arctan(1/Q_{13})/\pi$ , where  $Q_{13} = 2Q_{33}/(\delta_Q C_{33}^2/C_{13}^2 + 2)$  (i.e.,  $M_{13}$  is defined under acoustic approximation). Thereafter, Eq. (10) can be expressed as

$$V_p^2(\theta) = M_{11} \sin^2 \theta + M_{33} \cos^2 \theta + \frac{[M_{13}^2/M_{33} - M_{11}] \sin^2 \theta \cos^2 \theta}{[(1 + 2\epsilon)\sin^2 \theta + \cos^2 \theta] - 2(\epsilon - \delta)\sin^2 \theta \cos^2 \theta} \quad (11)$$

The accuracy analysis of Eq. (11) are presented in section 2.2. Additionally, we can rewrite Eq. (11) as

$$\omega^2 = \left( \eta_{11} k_x^{2\gamma_{11}} + \tau_{11}(i\omega) k_x^{2\gamma_{11}-1} \right) k_x^2 + \left( \eta_{33} k_z^{2\gamma_{33}} + \tau_{33}(i\omega) k_z^{2\gamma_{33}-1} \right) k_z^2 + \frac{[a_3 k_x^{2\lambda_{13}} + b_3(i\omega) k_x^{2\lambda_{13}-1}] - [\eta_{11} k_x^{2\gamma_{11}} + \tau_{11}(i\omega) k_x^{2\gamma_{11}-1}]}{[(1 + 2\epsilon)k_x^4 + k_z^4 + 2(1 + \delta)k_x^2 k_z^2]} \quad (19)$$

$$V_p^2(\theta) = M_{11} \sin^2 \theta + M_{33} \cos^2 \theta + \frac{[M_{13}^2/M_{33} - M_{11}] \sin^2 \theta \cos^2 \theta (\sin^2 \theta + \cos^2 \theta)}{[(1 + 2\epsilon)\sin^2 \theta + \cos^2 \theta] (\sin^2 \theta + \cos^2 \theta) - 2(\epsilon - \delta)\sin^2 \theta \cos^2 \theta} \quad (12)$$

In VTI media, the relation between phase velocity, frequency and wavenumber is given as shown below (Zhan et al., 2012):

$$\sin \theta = \frac{V_p(\theta) k_x}{\omega}, \cos \theta = \frac{V_p(\theta) k_z}{\omega}, \quad (13)$$

where  $k_x, k_z$  denote  $x, z$  direction wavenumber, respectively. Substituting Eq. (13) into Eq. (12), Eq. (12) can be written as

$$\omega^2 = M_{11} k_x^2 + M_{33} k_z^2 + \frac{(M_{13}^2/M_{33} - M_{11}) k_x^2 k_z^2 (k_x^2 + k_z^2)}{[(1 + 2\epsilon)k_x^4 + k_z^4 + 2(1 + \delta)k_x^2 k_z^2]} \quad (14)$$

The term  $(i\omega)^{2\gamma_{ij}}$  in Eq. (14) can be converted into fractional Laplacians to reduce the computational memory (Zhu and Harris, 2014), which can be expressed as

$$(i\omega)^{2\gamma_{ij}} \approx v^{2\gamma_{ij}} k^{2\gamma_{ij}} \cos(\pi\gamma_{ij}) + i\omega v^{2\gamma_{ij}-1} k^{2\gamma_{ij}-1} \sin(\pi\gamma_{ij}), \quad (15)$$

where  $k$  is the spatial wavenumber,  $v$  denotes the phase velocity at the reference frequency. Note that the phase velocity  $v$  is replaced by  $v_{11} = v_p \sqrt{(1 + 2\epsilon)}$ ,  $v_{33} = v_p$ , and  $v_{13} = v_p(1 + 2\delta)^{1/4}$  in the process of solving  $M_{11}$ ,  $M_{33}$ , and  $M_{13}$  (Qiao et al., 2020), respectively.  $v_p$  denotes the P-wave velocity along the vertical symmetry axis at the reference frequency. Using Eq. (15),  $M_{ij}$  can be written as

$$M_{ij} \approx \eta_{ij} k^{2\gamma_{ij}} + i\omega \tau_{ij} k^{2\gamma_{ij}-1}, \quad (16)$$

where

$$\eta_{ij} = C_{ij}^{\gamma_{ij}+1} \cos^2(\pi\gamma_{ij}/2) \omega_0^{-2\gamma_{ij}} \cos(\pi\gamma_{ij}), \quad (17)$$

$$\tau_{ij} = C_{ij}^{\gamma_{ij}+0.5} \cos^2(\pi\gamma_{ij}/2) \omega_0^{-2\gamma_{ij}} \sin(\pi\gamma_{ij}). \quad (18)$$

Inserting Eq. (16) into Eq. (14), we derive the pure-viscoacoustic dispersion relation in VTI media:

where  $\lambda_{13} = 2\gamma_{13} - \gamma_{33}$ ,  $a_3 = (C_{13}^2/C_{33})^{\lambda_{13}+1} \cos^2(\pi\lambda_{13}/2) \omega_0^{-2\lambda_{13}} \cos(\pi\lambda_{13})$ ,  $b_3 = (C_{13}^2/C_{33})^{\lambda_{13}+0.5} \cos^2(\pi\lambda_{13}/2) \omega_0^{-2\lambda_{13}} \sin(\pi\lambda_{13})$ ,  $\eta_{11} = C_{11}^{\gamma_{11}+1} \cos^2(\pi\gamma_{11}/2) \omega_0^{-2\gamma_{11}} \cos(\pi\gamma_{11})$ ,  $\tau_{11} = C_{11}^{\gamma_{11}+0.5} \cos^2(\pi\gamma_{11}/2) \omega_0^{-2\gamma_{11}} \sin(\pi\gamma_{11})$ ,  $\eta_{33} = C_{33}^{\gamma_{33}+1} \cos^2(\pi\gamma_{33}/2) \omega_0^{-2\gamma_{33}} \cos(\pi\gamma_{33})$ ,  $\tau_{33} = C_{33}^{\gamma_{33}+0.5} \cos^2(\pi\gamma_{33}/2) \omega_0^{-2\gamma_{33}} \sin(\pi\gamma_{33})$ .

By transforming Eq. (19) into the time-space domain, we can obtain the time-space domain pure-viscoacoustic VTI wave equation as follows:

$$\frac{\partial^2 p}{\partial t^2} = \left( \eta_{11} (-\nabla^2)^{\gamma_{11}} + \tau_{11} \frac{\partial}{\partial t} (-\nabla^2)^{\gamma_{11}-0.5} \right) \frac{\partial^2 p}{\partial x^2} + \left( \eta_{33} (-\nabla^2)^{\gamma_{33}} + \tau_{33} \frac{\partial}{\partial t} (-\nabla^2)^{\gamma_{33}-0.5} \right) \frac{\partial^2 p}{\partial z^2} + \left[ \left( a_3 (-\nabla^2)^{\lambda_{13}} + b_3 \frac{\partial}{\partial t} (-\nabla^2)^{\lambda_{13}-0.5} \right) - \left( \eta_{11} (-\nabla^2)^{\gamma_{11}} + \tau_{11} \frac{\partial}{\partial t} (-\nabla^2)^{\gamma_{11}-0.5} \right) \right] \frac{\partial^4}{\partial x^2 \partial z^2} \left( \frac{\partial^2}{\partial x^2} + \frac{\partial^2}{\partial z^2} \right) p + f, \tag{20}$$

$$\left[ (1 + 2\varepsilon) \frac{\partial^4}{\partial x^4} + \frac{\partial^4}{\partial z^4} + 2(1 + \delta) \frac{\partial^4}{\partial x^2 \partial z^2} \right]$$

where  $f$  is source function. We notice that Eq. (20) is equivalent to the time-space domain anisotropic pure P-wave equation given by Liang et al. (2023) when  $Q_p \rightarrow \infty$ .

In TTI media, the pure-viscoacoustic TTI wave equation can be deduced from Eq. (20) through coordinate rotation. The wavenumber relationship between VTI and TTI media (Zhan et al., 2012) can be expressed as

$$\begin{aligned} \hat{k}_x &= \cos \varphi k_x - \sin \varphi k_z, \\ \hat{k}_z &= \sin \varphi k_x + \cos \varphi k_z, \end{aligned} \tag{21}$$

where

$$S_k = \frac{(\cos \varphi k_x - \sin \varphi k_z)^2 (\sin \varphi k_x + \cos \varphi k_z)^2}{\left[ (1 + 2\varepsilon) (\cos \varphi k_x - \sin \varphi k_z)^4 + (\sin \varphi k_x + \cos \varphi k_z)^4 + 2(1 + \delta) (\cos \varphi k_x - \sin \varphi k_z)^2 (\sin \varphi k_x + \cos \varphi k_z)^2 \right]}. \tag{23}$$

Multiplying both sides of Eq. (22) with the wavefield  $p(\omega, k_x, k_z)$ , and applying the inverse Fourier transforms relations  $\omega^2 \rightarrow \partial^2 / \partial t^2$ ,  $k_x^2 \rightarrow \partial^2 / \partial x^2$ ,  $k_z^2 \rightarrow \partial^2 / \partial z^2$ . Then, the time-space domain pure-viscoacoustic TTI wave equation can be expressed as

$$\begin{aligned} \frac{\partial^2 p}{\partial t^2} &= \left( \eta_{11} (-\nabla^2)^{\gamma_{11}} + \tau_{11} \frac{\partial}{\partial t} (-\nabla^2)^{\gamma_{11}-0.5} \right) \left( \cos^2 \varphi \frac{\partial^2}{\partial x^2} + \sin^2 \varphi \frac{\partial^2}{\partial z^2} - \sin(2\varphi) \frac{\partial^2}{\partial x \partial z} \right) p + \\ &\left( \eta_{33} (-\nabla^2)^{\gamma_{33}} + \tau_{33} \frac{\partial}{\partial t} (-\nabla^2)^{\gamma_{33}-0.5} \right) \left( \sin^2 \varphi \frac{\partial^2}{\partial x^2} + \cos^2 \varphi \frac{\partial^2}{\partial z^2} + \sin(2\varphi) \frac{\partial^2}{\partial x \partial z} \right) p + \\ &\left[ \left( a_3 (-\nabla^2)^{\lambda_{13}} + b_3 \frac{\partial}{\partial t} (-\nabla^2)^{\lambda_{13}-0.5} \right) - \left( \eta_{11} (-\nabla^2)^{\gamma_{11}} + \tau_{11} \frac{\partial}{\partial t} (-\nabla^2)^{\gamma_{11}-0.5} \right) \right] S_t \left( \frac{\partial^2}{\partial x^2} + \frac{\partial^2}{\partial z^2} \right) p + f, \end{aligned} \tag{24}$$

where

$$S_t = \frac{\left( \cos^2 \varphi \sin^2 \varphi \left( \frac{\partial^4}{\partial x^4} + \frac{\partial^4}{\partial z^4} \right) + \left( \cos^4 \varphi + \sin^4 \varphi - \sin^2(2\varphi) \right) \frac{\partial^4}{\partial x^2 \partial z^2} \right) + \cos(2\varphi) \sin(2\varphi) \frac{\partial^4}{\partial x^3 \partial z} - \cos(2\varphi) \sin(2\varphi) \frac{\partial^4}{\partial x \partial z^3}}{\left( 2\varepsilon \cos^4 \varphi + 2\delta \cos^2 \varphi \sin^2 \varphi \right) \frac{\partial^4}{\partial x^4} + \left( 2\varepsilon \sin^4 \varphi + 2\delta \cos^2 \varphi \sin^2 \varphi \right) \frac{\partial^4}{\partial z^4} + 3(\varepsilon - \delta) \sin^2(2\varphi) \frac{\partial^4}{\partial x^2 \partial z^2} + \left( 2\delta \cos(2\varphi) - 4\varepsilon \cos^2 \varphi \right) \sin(2\varphi) \frac{\partial^4}{\partial x^3 \partial z} - \left( 4\varepsilon \sin^2 \varphi + 2\delta \cos(2\varphi) \right) \sin(2\varphi) \frac{\partial^4}{\partial x \partial z^3}}. \tag{25}$$

where  $\varphi$  denotes the dip angle of the symmetry axis. Replacing  $k_x$  and  $k_z$  in Eq. (19) with  $\hat{k}_x$  and  $\hat{k}_z$ , Eq. (20) can be written as

$$\begin{aligned} \omega^2 &= \left( \eta_{11} k^2 \gamma_{11} + \tau_{11} (i\omega) k^{2\gamma_{11}-1} \right) \left( \cos^2 \varphi k_x^2 + \sin^2 \varphi k_z^2 - \sin(2\varphi) k_x k_z \right) + \\ &\left( \eta_{33} k^2 \gamma_{33} + \tau_{33} (i\omega) k^{2\gamma_{33}-1} \right) \left( \sin^2 \varphi k_x^2 + \cos^2 \varphi k_z^2 + \sin(2\varphi) k_x k_z \right) + \\ &\left[ \left( a_3 k^{2\lambda_{13}} + b_3 (i\omega) k^{2\lambda_{13}-1} \right) - \left( \eta_{11} k^2 \gamma_{11} + \tau_{11} (i\omega) k^{2\gamma_{11}-1} \right) \right] S_k \left( k_x^2 + k_z^2 \right), \end{aligned} \tag{22}$$

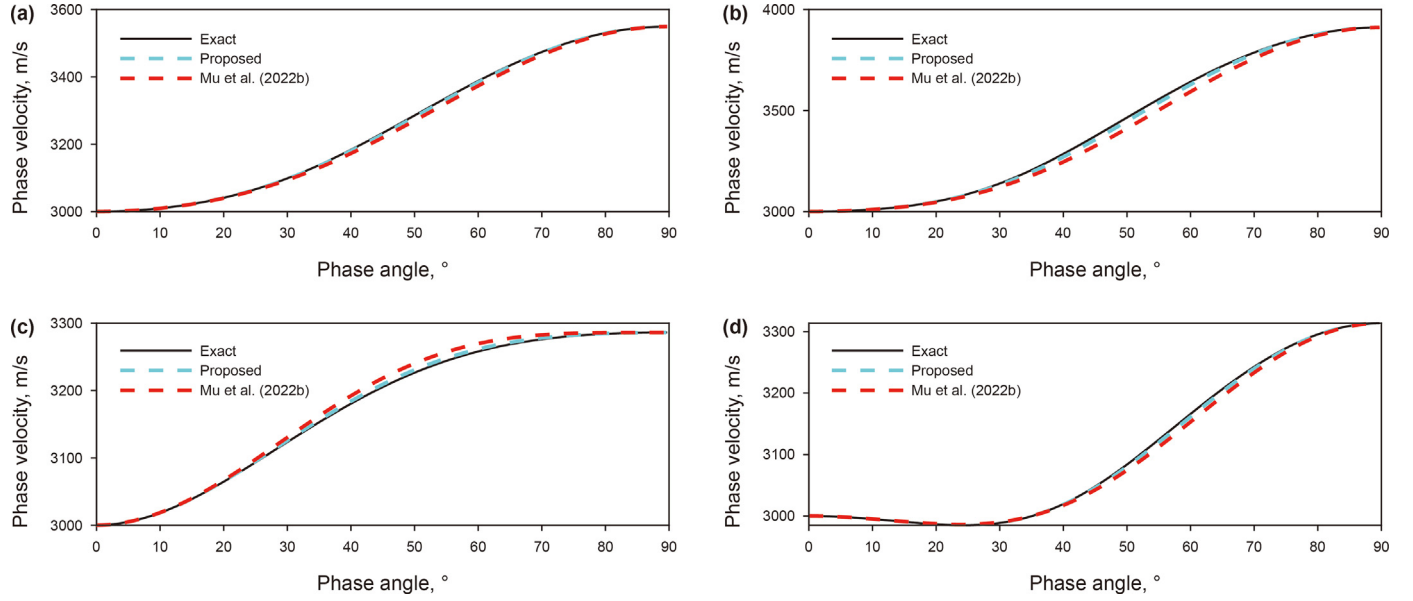


**Fig. 1.** The comparisons of the P-wave phase velocity curves for different media parameters. The black solid lines, the cyan dashed lines, and the red dashed lines denote the exact phase velocity formula of P-wave in viscoelastic VTI media, our approximate formula and the approximate formula given by Mu et al. (2022b), respectively. The media parameters from (a) to (d) are Model A to Model D in Table 1, respectively.

It is notable that Eq. (24) contains decoupled phase dispersion terms and amplitude attenuation terms. In the above equations, the phase dispersion effects are dominated by a term containing  $(-\nabla^2)^{\gamma_{ij}}$ , the amplitude attenuation effects are dominated by a term containing  $\partial(-\nabla^2)^{\gamma_{ij}-0.5}/\partial t$ . If we only consider phase dispersion effects, the dispersion-dominated wave equation can be given as

$$\begin{aligned} \frac{\partial^2 p}{\partial t^2} &= \eta_{11} (-\nabla^2)^{\gamma_{11}} \left( \cos^2 \varphi \frac{\partial^2}{\partial x^2} + \sin^2 \varphi \frac{\partial^2}{\partial z^2} - \sin(2\varphi) \frac{\partial^2}{\partial x \partial z} \right) p + \\ &\eta_{33} (-\nabla^2)^{\gamma_{33}} \left( \sin^2 \varphi \frac{\partial^2}{\partial x^2} + \cos^2 \varphi \frac{\partial^2}{\partial z^2} + \sin(2\varphi) \frac{\partial^2}{\partial x \partial z} \right) p + \\ &\left( \eta_3 (-\nabla^2)^{\lambda_{13}} - \eta_{11} (-\nabla^2)^{\gamma_{11}} \right) S_t \left( \frac{\partial^2}{\partial x^2} + \frac{\partial^2}{\partial z^2} \right) p + f. \end{aligned} \tag{26}$$

Similarly, the dissipation-dominated wave equation can be written as

$$\begin{aligned} \frac{\partial^2 p}{\partial t^2} &= \left( C_{11} + \tau_{11} \frac{\partial}{\partial t} (-\nabla^2)^{\gamma_{11}-0.5} \right) \left( \cos^2 \varphi \frac{\partial^2}{\partial x^2} + \sin^2 \varphi \frac{\partial^2}{\partial z^2} - \sin(2\varphi) \frac{\partial^2}{\partial x \partial z} \right) p + \\ &\left( C_{33} + \tau_{33} \frac{\partial}{\partial t} (-\nabla^2)^{\gamma_{33}-0.5} \right) \left( \sin^2 \varphi \frac{\partial^2}{\partial x^2} + \cos^2 \varphi \frac{\partial^2}{\partial z^2} + \sin(2\varphi) \frac{\partial^2}{\partial x \partial z} \right) p + \\ &\left[ \left( C_{13}^2 / C_{33} + \tau_{33} \frac{\partial}{\partial t} (-\nabla^2)^{\lambda_{13}-0.5} \right) - \left( C_{11} + \tau_{11} \frac{\partial}{\partial t} (-\nabla^2)^{\gamma_{11}-0.5} \right) \right] S_t \left( \frac{\partial^2}{\partial x^2} + \frac{\partial^2}{\partial z^2} \right) p + f. \end{aligned} \tag{27}$$

### 2.2. Theoretical accuracy analysis of the proposed pure-viscoacoustic TTI wave equation

In this section, several theoretical analysis experiments are performed to investigate the accuracy of the newly proposed wave equation. The comparisons between the exact complex-valued phase velocity formula for P-wave in viscoelastic TTI media (Eq. (A-1)), the formula proposed by Mu et al. (2022b), and our formula are generated for accuracy analysis. First, we plot the phase velocity curves for different parameters shown in Fig. 1, the model parameters are given in Table 1. Note that the phase velocity can be generated using Eq. (A-3). The source dominant frequency is the same as the reference frequency, which is 30 Hz.

Fig. 1 shows that the phase velocity curves of the proposed formula (Eq. (24)) are in better match with the phase velocity curves of exact formula than that of the formula given by Mu et al. (2022b). With velocity anisotropy strengthening, the newly derived formula is more accurate than the formula of Mu et al. (2022b), as shown in Fig. 1(b). These results suggest that the newly derived formula has higher accuracy than the formula derived by Mu et al. (2022b).

Furthermore, we generate the maximum relative error to

**Table 1**

The model parameters for VTI models to generate the phase velocity curve for accuracy analysis (The parameters  $v_s$  and  $Q_s$  are the SV-wave velocity and quality factor, which is used for generating the exact complex-valued phase velocity for P-wave in viscoelastic anisotropic media.)

Model	Model parameters							
	$v_p, \text{m/s}$	$v_s, \text{m/s}$	$\epsilon$	$\delta$	$\epsilon_Q$	$\delta_Q$	$Q_p$	$Q_s$
<b>Model A</b>	3000	1800	0.2	0.1	-0.4	-0.3	30	20
<b>Model B</b>	3000	1800	0.35	0.1	-0.7	-0.3	30	20
<b>Model C</b>	3000	1800	0.1	0.2	-0.2	-0.6	30	20
<b>Model D</b>	3000	1800	0.11	-0.055	-0.3	-0.15	30	20

investigate the accuracy of the newly derived wave equation. The maximum relative error function given by Mu et al. (2020) can be reformulated as

$$E_R(x, y) = \max\left(\frac{|V_e(x, y, \theta) - V_a(x, y, \theta)|}{V_a(x, y, \theta)}\right), \theta \in \left(0, \frac{\pi}{2}\right), \quad (28)$$

where  $V_e(x, y, \theta)$  denotes the exact formula of P-wave in viscoelastic anisotropic media;  $V_a(x, y, \theta)$  represents the approximate P-wave formula in viscoacoustic anisotropic media;  $x$  and  $y$  denote the variable we are studying. Fig. 2(a)–(b) shows the maximum relative error of the phase velocity of different approximate formulas. Fig. 2(c)–(d) shows the maximum relative error of the quality of different approximate formulas. The phase velocity and quality factor can be generated using Eq. (A-3) and Eq. (A-4), respectively. In Fig. 2(a)–(b), the proposed formula has more area with relative phase velocity error less than 1%, in comparison to the formula proposed by Mu et al. (2022b). This result suggests that the newly derived equation has higher accuracy in representing velocity

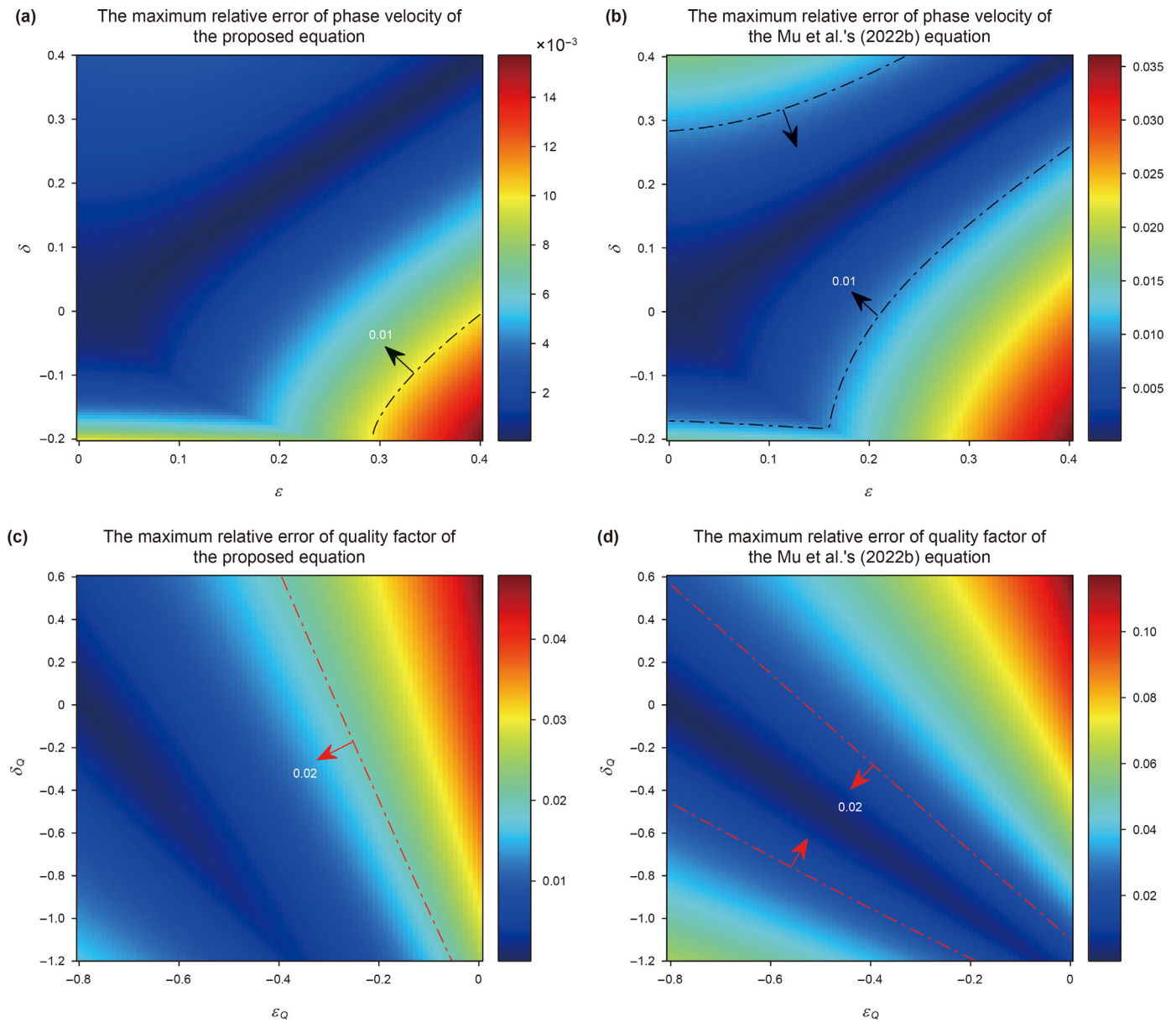


**Fig. 2.** The maximum relative error of the phase velocity and quality factor of the different approximation formulas. (a) and (b) are the maximum relative error of the phase velocity; (c) and (d) are the maximum relative error of the quality factor. The attenuation anisotropy parameters of (a) and (b) are  $\epsilon_Q = -0.4$ ,  $\delta_Q = -0.3$ . The velocity anisotropy parameters of (c) and (d) are  $\epsilon = 0.15$ ,  $\delta = 0.1$ . The P-wave model parameters are  $v_p = 3000 \text{ m/s}$ ,  $Q_p = 30$ , and the parameters  $v_s = 1800 \text{ m/s}$  and  $Q_s = 20$  are for viscoelastic anisotropic media.

anisotropy than the formula given by Mu et al. (2022b). Moreover, from Fig. 2(c)–(d), one can clearly see that the maximum relative error of quality factor of the proposed formula is obvious smaller than the formula proposed by Mu et al. (2022b), which demonstrates the proposed formula with higher precision in representing attenuation anisotropy. From the above results, one can conclude that the newly derived equation has higher accuracy than the formula developed by Mu et al. (2022b) in describing velocity anisotropy and attenuation anisotropy.

### 3. Numerical implementations

In this section, we develop the HFDLRD method to accurately solve our new wave equation. The variable-order fractional Laplacians and mixed-domain operator  $S_k$  are solved by the low-rank decomposition method (Sun et al., 2016), and the other partial derivatives are solved by the finite-difference method. The low-rank decomposition method was developed by Fomel et al. (2013), which can be expressed as

$$W(\mathbf{x}, \mathbf{k}) \approx \sum_{m=1}^M W_1(\mathbf{x}, \mathbf{k}_m) \sum_{n=1}^N a_{mn} W_2(\mathbf{x}_n, \mathbf{k}), \quad (29)$$

where  $W_1(\mathbf{x}, \mathbf{k}_m)$  and  $W_2(\mathbf{x}_n, \mathbf{k})$  are the submatrices of  $W(\mathbf{x}, \mathbf{k})$ , which are related to the wavenumbers and spatial locations, respectively. The coefficient  $a_{mn}$  is the connection between  $W_1(\mathbf{x}, \mathbf{k}_m)$  and  $W_2(\mathbf{x}_n, \mathbf{k})$ , and  $m$  and  $n$  is the rank of the matrixes. In addition, the coefficient  $a_{mn}$  can be determined using expression that  $a_{mn} = W^\dagger(\mathbf{x}_n, \mathbf{k}_m)$ , where  $\dagger$  denotes the pseudoinverse (seen more detail in Fomel et al., 2013). Based on the HFDLRD strategy, Eq. (24) can be rewritten as

$$\begin{aligned} \frac{\partial^2 p}{\partial t^2} &= (a_{11}q_1 + b_{11}q_2) \left( \cos^2 \varphi \frac{\partial^2}{\partial x^2} + \sin^2 \varphi \frac{\partial^2}{\partial z^2} - \sin 2\varphi \frac{\partial^2}{\partial x \partial z} \right) + \\ &(a_{33}q_3 + b_{33}q_4) \left( \sin^2 \varphi \frac{\partial^2}{\partial x^2} + \cos^2 \varphi \frac{\partial^2}{\partial z^2} + \sin 2\varphi \frac{\partial^2}{\partial x \partial z} \right) + \\ &(a_3q_5 + b_3q_6 - (a_{11}q_7 + b_{11}q_8)) \left( \frac{\partial^2}{\partial x^2} + \frac{\partial^2}{\partial z^2} \right) + f, \end{aligned} \quad (30)$$

where  $q_1 = \mathcal{F}^{-1}(k^{2\gamma_{11}} \mathcal{F}(p))$ ,  $q_2 = \mathcal{F}^{-1}(k^{2\gamma_{11}-1} \mathcal{F}(\partial p / \partial t))$ ,  $q_3 = \mathcal{F}^{-1}(k^{2\gamma_{33}} \mathcal{F}(p))$ ,  $q_4 = \mathcal{F}^{-1}(k^{2\gamma_{33}-1} \mathcal{F}(\partial p / \partial t))$ ,  $q_5 = \mathcal{F}^{-1}(k^{2\gamma_{13}} S_k \mathcal{F}(p))$ ,  $q_6 = \mathcal{F}^{-1}(k^{2\gamma_{13}-1} S_k \mathcal{F}(\partial p / \partial t))$ ,  $q_7 = \mathcal{F}^{-1}(k^{2\gamma_{11}} S_k \mathcal{F}(p))$ ,  $q_8 = \mathcal{F}^{-1}(k^{2\gamma_{11}-1} S_k \mathcal{F}(\partial p / \partial t))$ .  $\mathcal{F}$  and  $\mathcal{F}^{-1}$  denote the forward fast Fourier transforms (FFTs) and inverse FFTs, respectively. Based on Eq. (28),  $q_1$  can be solved by the low-rank decomposition as follows:

$$\mathcal{F}^{-1} \left( \left( -\nabla^2 \right)^{\gamma_{11}} \mathcal{F}(p) \right) \approx \sum_{m=1}^M W_1(\mathbf{x}, \mathbf{k}_m) \left( \sum_{n=1}^N a_{mn} \mathcal{F}^{-1}(W_2(\mathbf{x}_n, \mathbf{k}) \mathcal{F}(p)) \right). \quad (31)$$

Correspondingly,  $q_2 - q_8$  also can be solved by the low-rank decomposition method. To solve Eq. (31), we can use a small rank of low-rank decomposition to meet the accuracy requirement well, because Eq. (31) is independent by the velocity model (Yan and Liu,

2016; Zhang et al., 2019). Here, if the ranks of the low-rank decomposition in solving  $q_1 - q_4$  and  $q_5 - q_8$  are defined as  $N_1$  and  $N_2$  respectively, then, the number of forward FFTs and inverse FFTs are 2 and  $4N_1 + 4N_2$  respectively.

### 4. Numerical examples

In this section, we use several homogeneous and heterogeneous models to illustrate the accuracy and stability of our proposed pure-viscoacoustic TTI wave equation (Eq. (24)). The coupled pseudo-viscoacoustic TTI wave equation derived by Qiao et al. (2020) is used as the reference to evaluate the accuracy of the newly derived equation, due to the wavefield simulated by the coupled pseudo-viscoacoustic TTI wave equation preserves accurately the kinematic features (Mu et al., 2022b). For numerical implementation, all the numerical examples used in this section are solved by the HFDLRD method. In addition, the density is uniformly defined as  $\rho = 1$  in all numerical examples. A simple two-layer model is employed to investigate the accuracy of the proposed HFDLRD method. The boundary reflections are attenuated by using the sponge absorbing boundary (Cerjan et al., 1985).

#### 4.1. A homogeneous model

##### 4.1.1. Accuracy analysis of the proposed pure-viscoacoustic TTI wave equation

In this case, we build a homogeneous model to perform wavefield simulation to illustrate the accuracy of our new pure-viscoacoustic TTI wave equation. The homogeneous model is built of  $401 \times 401$  grids and discretized with grid spacing of  $10 \text{ m} \times 10 \text{ m}$ . A Ricker wavelet with the dominant frequency of 25 Hz is injected at the central of model; the time step is 0.001 s; the reference frequency is 25 Hz. Fig. 3 shows the snapshots at 0.5 s for different attenuating VTI models simulated by the coupled pseudo-viscoacoustic TTI wave equation of Qiao et al. (2020), the pure-viscoacoustic TTI wave equation derived by Mu et al. (2022b), and our new wave equation, respectively. The ranks of the low-rank decomposition method are  $N_1 = 1$  and  $N_2 = 1$ .

From Fig. 3, one can observe that the wavefields generated by the coupled pseudo-viscoacoustic TTI wave equation produce the S-wave artifacts, while the wavefields generated by the pure-viscoacoustic TTI wave equation are free of S-wave artifacts. This result suggests that the wavefields simulated by pure-viscoacoustic TTI wave equation are noise-free. Additionally, Figs. (4) and (5) show the wavefield snapshots comparison in a wiggle format. Fig. 4(a) is the superposition of Fig. 3(e) (red dashed line) and Fig. 3(d) (black solid line). Fig. 4(b) is the superposition of Fig. 3(f) (red dashed line) and Fig. 3(d) (black solid line). Similarly, Fig. 5(a) is the superposition of Fig. 3(h) (red dashed line) and Fig. 3(g) (black solid line). Fig. 5(b) is the superposition of Fig. 3(i) (red dashed line) and Fig. 3(g) (black solid line). Given that the attenuation param-

eters in Fig. 3(d)–(e) are set as isotropy, Fig. 4 can be used to investigate the accuracy of our new wave equation in representing velocity anisotropy. Fig. 4 clearly shows that the wavefields generated by the newly derived wave equation are in better

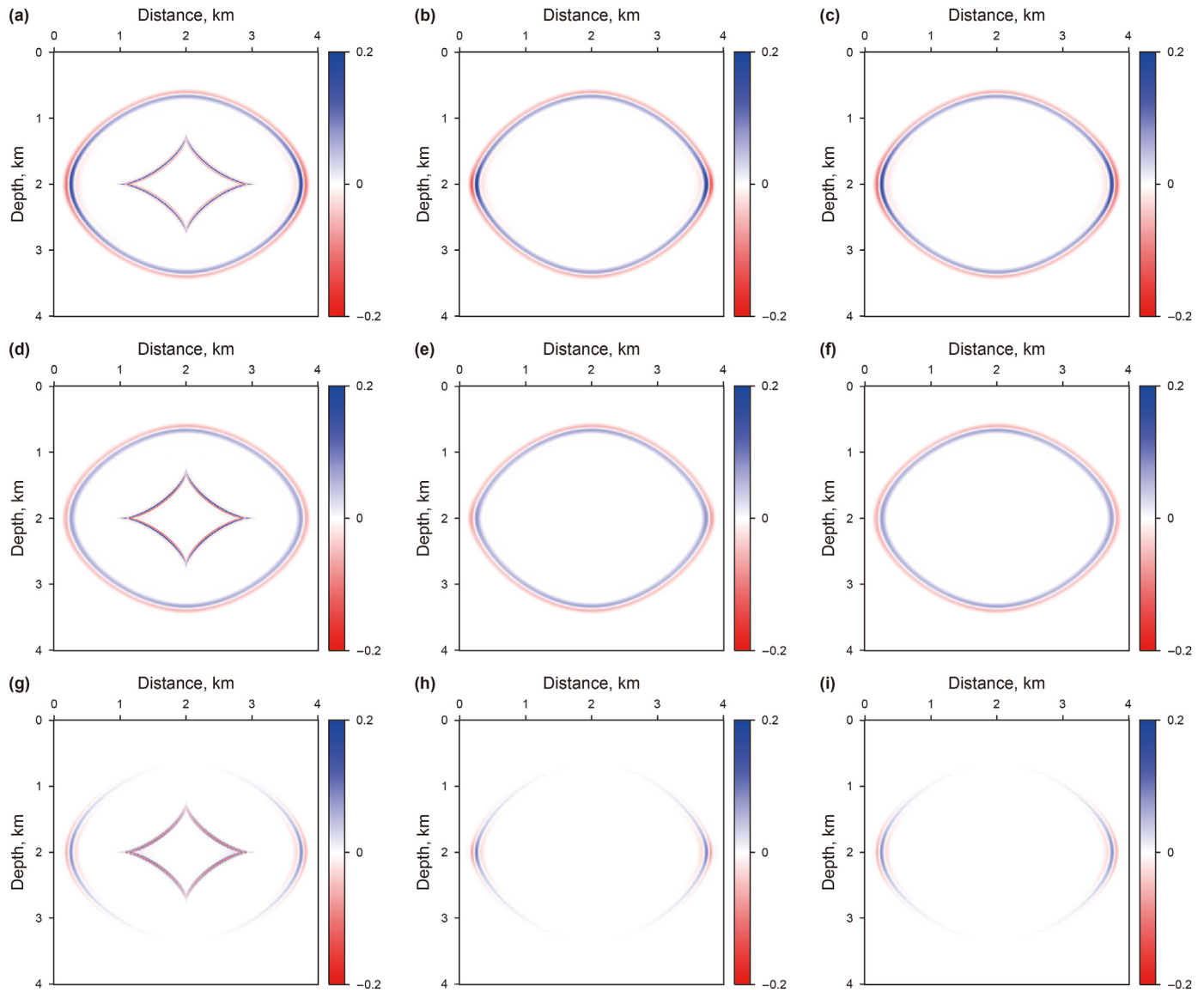


**Fig. 3.** Wavefield snapshots at 0.5 s for different attenuating VTI models. The same parameters for these VTI models are:  $v_p = 3000$  m/s,  $\epsilon = 0.35$ ,  $\delta = 0.05$ ,  $\varphi = 0$ ,  $Q_p = 30$ . The attenuation anisotropy parameters are: (a)–(c)  $\epsilon_Q = -0.7$ ,  $\delta_Q = -0.15$ ; (d)–(f)  $\epsilon_Q = 0$ ,  $\delta_Q = 0$ . (g) is the difference between (a) and (d), (h) is the difference between (b) and (e), and (i) is the difference between (c) and (f). The first column to the third column are the wavefields simulated by the coupled pseudo-viscoacoustic TTI wave equation derived by Qiao et al. (2020), the pure-viscoacoustic TTI wave equation proposed by Mu et al. (2022b), and our new pure-viscoacoustic TTI wave equation, respectively.

agreement with the reference traces (black line) than the wavefields simulated by the pure-viscoacoustic TTI wave equation derived by Mu et al. (2022b), as pointed out by the black arrows. This result illustrates that the newly derived wave equation has higher accuracy in describing velocity anisotropy than the pure-viscoacoustic TTI wave equation proposed by Mu et al. (2022b). Similar with Fig. 4, the results in Fig. 5 show that the wavefields calculated by the proposed wave equation are closer to the reference wavefields than that of the pure-viscoacoustic TTI wave equation given by Mu et al. (2022b). This finding demonstrates that the wavefields simulated by our new wave equation are more accurate than the pure-viscoacoustic TTI wave equation derived by Mu et al. (2022b) in representing the attenuation anisotropy characteristics. Therefore, according to the above results, we can conclude that the newly derived wave equation has higher accuracy than the pure-viscoacoustic TTI wave equation proposed by Mu et al. (2022b) in describing velocity anisotropy and attenuation anisotropy. These numerical results also are consistent with the

theoretical analysis displayed in Figs. 1 and 2.

#### 4.1.2. Modeling of the decoupled amplitude attenuation and phase dispersion effects

To demonstrate the effects of decoupled amplitude attenuation and phase dispersion of our pure-viscoacoustic TTI wave equation, we build a homogenous model with grid points of  $401 \times 401$  and a spacing of 10 m. The model parameters are  $v_p = 3000$  m/s,  $\epsilon = 0.35$ ,  $\delta = 0.05$ ,  $\epsilon_Q = -0.7$ ,  $\delta_Q = -0.15$ ,  $\varphi = 45$ . The Ricker wavelet source with a dominant frequency of 25 Hz is located at the center of the model, besides, the time step is 0.001 s and the reference frequency is 1000 Hz. The ranks of the low-rank decomposition method are  $N_1 = 1$  and  $N_2 = 1$ . Fig. 6(a) displays wavefield snapshots at 0.5 s simulated by the different equations. In Fig. 6(a), comparing with the simulation results of the acoustic TTI equation, which can be found that the dissipation TTI equation decreases the amplitude energy, the dispersion equation mainly makes impact on phase delay, and the viscoacoustic TTI equation has influence both on

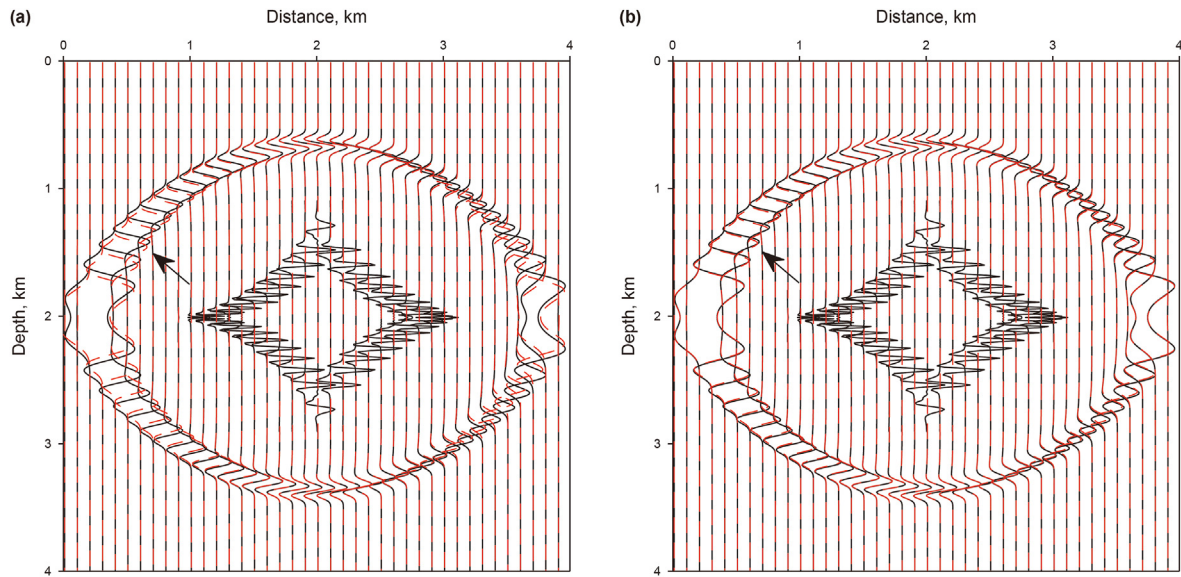


**Fig. 4.** Comparisons of wavefield snapshots from Fig. 3(d)–(f) in wiggle forms. (a) The wavefields generated by the pure-viscoacoustic TTI wave equation derived by Mu et al. (2022b) (Fig. 3(e)) (red dashed lines) and the reference wavefield (Fig. 3(d)) (black solid lines). (b) The wavefields generated by the proposed pure-viscoacoustic TTI wave equation (Fig. 3(f)) (red dashed lines) and the reference wavefield (Fig. 3(d)) (black solid lines).

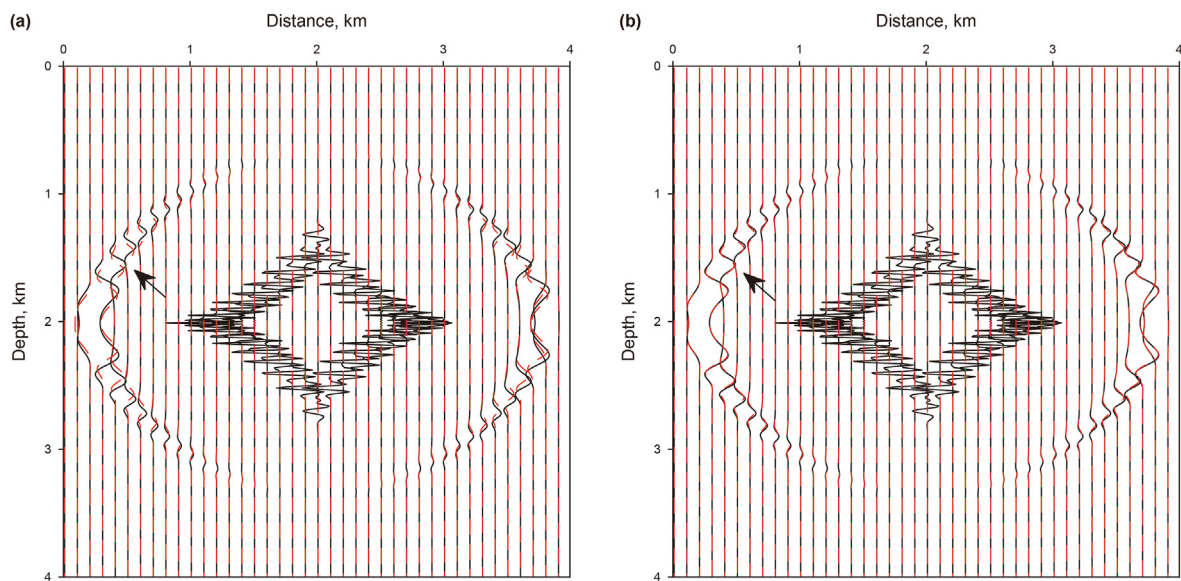


**Fig. 5.** Comparisons of wavefield snapshots from Fig. 3(g)–(i) in wiggle forms. (a) The wavefields generated by the pure-viscoacoustic TTI wave equation derived by Mu et al. (2022b) (Fig. 3(h)) (red dashed lines) and the reference wavefield (Fig. 3(g)) (black solid lines). (b) The wavefields generated by the proposed pure-viscoacoustic TTI wave equation (Fig. 3(i)) (red dashed lines) and the reference wavefield (Fig. 3(g)) (black solid lines).

amplitude decrease and phase delay. Fig. 6(b) shows wavefield snapshots at 0.5 s simulated by pure-viscoacoustic TTI wave equation with different quality factors, which illustrates that the lower the quality factor, amplitude attenuation and phase delay are more serious. The above results suggest that our pure-viscoacoustic anisotropic wave equation can achieve decoupled amplitude attenuation and phase dispersion wavefield simulations, which facilitate the realization of  $Q$ -compensated RTM in attenuating anisotropic media.

#### 4.2. A simple two-layer model

In this case, we use a simple two-layer model to investigate the

accuracy of the HFDRD method in solving the pure-viscoacoustic TTI wave equation. Note that the pure-viscoacoustic TTI wave equation proposed by Mu et al. (2022b) is used for generating wavefield in this case. The model is discretized with  $401 \times 401$  grid points uniformly along the vertical and horizontal directions with a spacing of 10 m. The source is a Ricker wavelet with a peak frequency of 25 Hz, which is placed at the central of model. The time step is 0.001 s and the reference frequency is 25 Hz. The reference wavefield is calculated by the blocked computing method (Li et al., 2016). We use the HFDRD method based on the second-order Taylor series expansion approximation of Zhang et al. (2020b) to generate wavefields for comparison. The ranks of the low-rank decomposition method are  $N_1 = 2$  and  $N_2 = 2$ . Wavefield snapshots at 0.9 s for

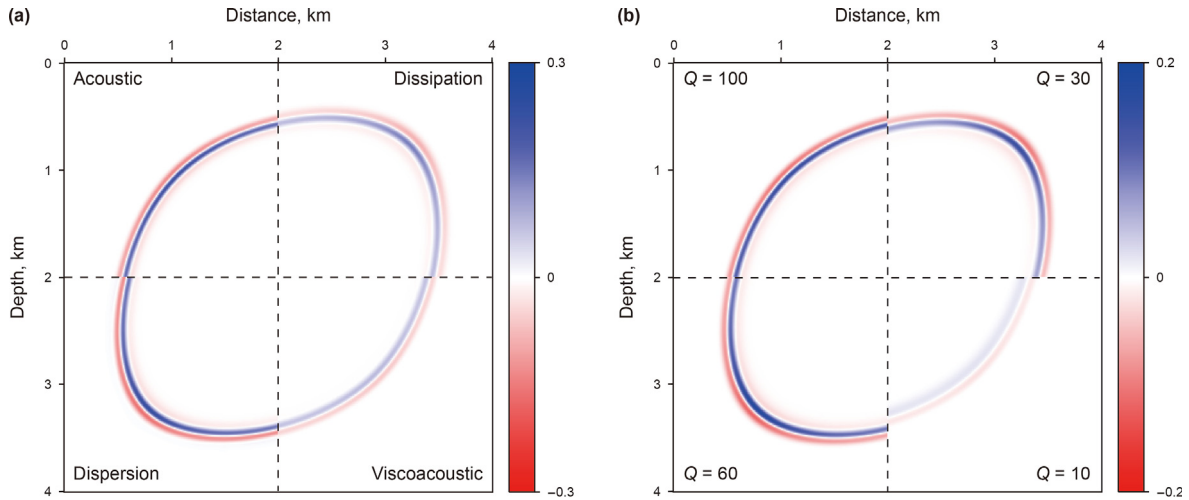


**Fig. 6.** Experiments of the newly proposed pure-viscoacoustic TTI wave equation simulating in the homogeneous media. (a) Wavefield snapshots at 0.5 s simulated by acoustic TTI, dissipation TTI, dispersion TTI, and viscoacoustic TTI wave equations. (b) Wavefield snapshots at 0.5 s simulated by pure-viscoacoustic TTI wave equation with different quality factor. The  $Q_p=30$  (in Fig. 6(a)), the reference frequency is 1000 Hz.

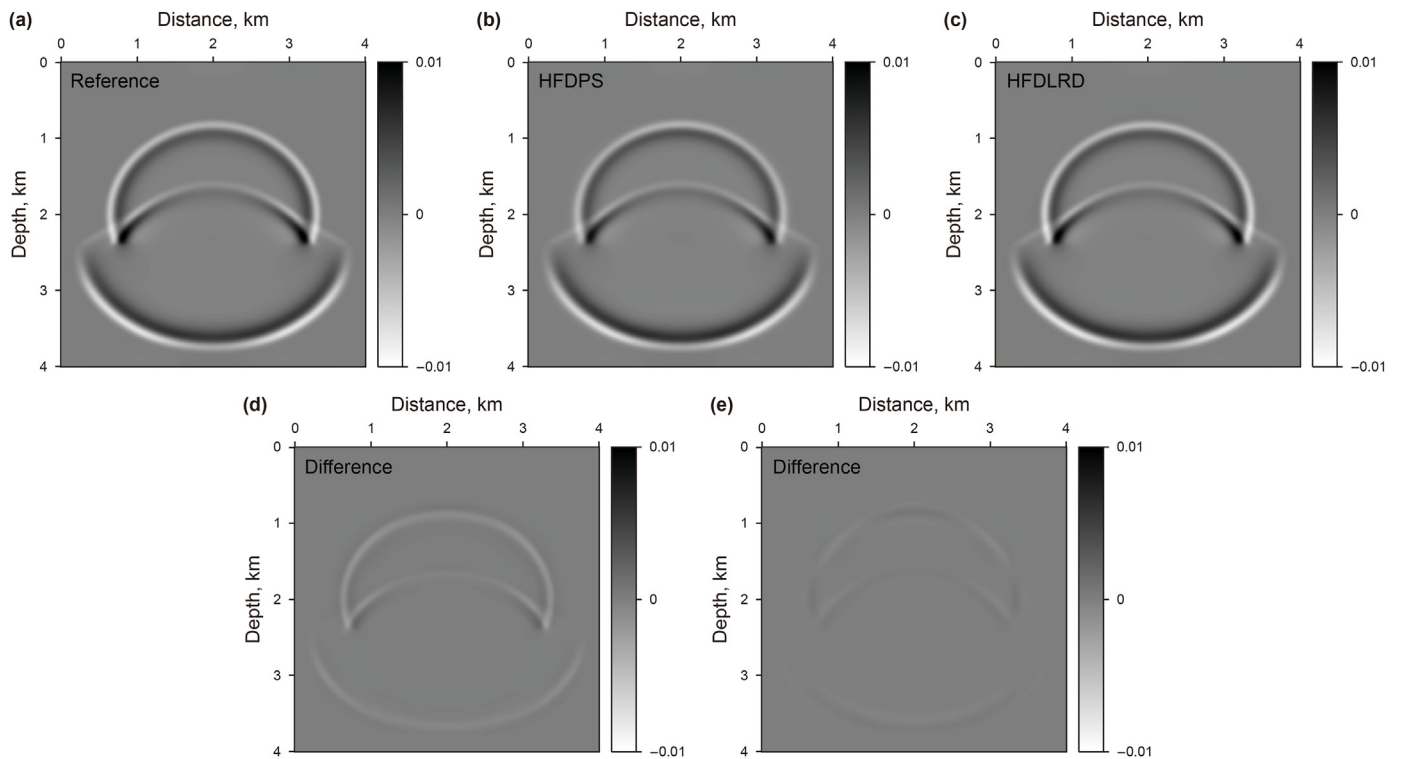


**Fig. 7.** Wavefield snapshots at 0.9 s computed using the block method (a), the HFDPs method (b), and the HFDLRD method (c), respectively. (d) and (e) show the differences between (b) and (a) and between (c) and (a), respectively. The first layer depth is 2.4 km and model parameters are  $v_p = 1500$  m/s,  $\epsilon = 0.15$ ,  $\delta = 0.1$ ,  $\epsilon_Q = -0.15$ ,  $\delta_Q = -0.3$ ,  $\varphi = 0$ ,  $Q_p = 5$ . The parameters of second layer are  $v_p = 2500$  m/s,  $\epsilon = 0.25$ ,  $\delta = 0.2$ ,  $\epsilon_Q = -0.25$ ,  $\delta_Q = -0.6$ ,  $\varphi = 0$ ,  $Q_p = 15$ .

the simple two-layer model calculated by the blocking method, the HFDPs method, and the HFDLRD method are shown in Fig. 7(a)–(c), respectively. The corresponding wavefield differences are shown in Fig. 7(d)–(e). From Fig. 7, one can see that the differences (Fig. 7(e)) between Fig. 7(a) and Fig. 7(c) are almost zero, while the differences (Fig. 7(d)) between Fig. 7(a) and Fig. 7(b) are apparent. The above findings suggest that HFDLRD method outperforms HFDPs method in terms of accuracy of wavefield simulation in attenuating anisotropic media, especially in the case of strong attenuation ( $Q < 10$ ).

#### 4.3. A modified Hess partial model

The modified complex Hess partial model is further used to verify the accuracy of the newly proposed equation simulated in complex media, and the model parameters are shown in Fig. 8. The model with size of 6 km  $\times$  3 km and discretized with grid spacing of 10 m  $\times$  10 m. A Ricker wavelet with a peak frequency of 20 Hz is located at (3000 m, 10 m). The time step is 0.001 s, the reference frequency is 20 Hz. The wavefield snapshots at 1.15 s generated by

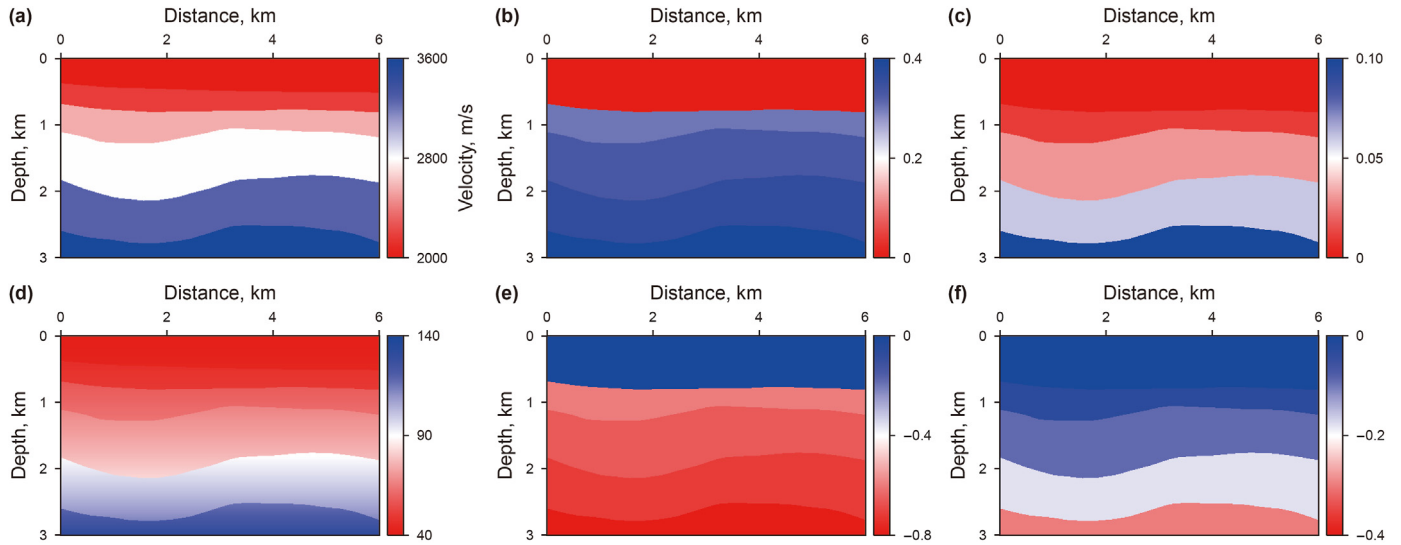


Fig. 8. Modified Hess partial model of velocity (a), Thomsen anisotropic parameters  $\epsilon$  (b) and  $\delta$  (c),  $Q_p$  (d),  $Q$ -related Thomsen anisotropic parameters  $\epsilon_Q$  (e) and  $\delta_Q$  (f).

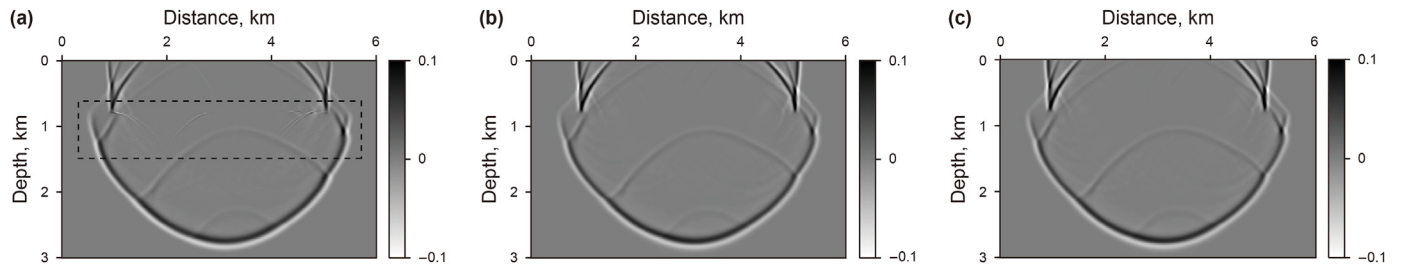


Fig. 9. Wavefield snapshots at 1.15 s generated by the coupled pseudo-viscoacoustic TTI wave equation derived by Qiao et al. (2020) (a), our pure-viscoacoustic TTI wave equation (b), the pure-viscoacoustic TTI wave equation derived by Mu et al. (2022b) (c), respectively.

different equations are shown in Fig. 9. The ranks of the low-rank decomposition method are  $N_1 = 2$  and  $N_2 = 2$ . In Fig. 9(a), there are shear wave artifacts in the wavefields (as shown in the black dashed rectangular box), while the wavefields simulated by pure-viscoacoustic TTI wave equation doesn't contain (as shown in Fig. 9(b)–(c)), which illustrates that pure-viscoacoustic TTI wave equation can obtain cleaner results than coupled pseudo-viscoacoustic TTI wave equation. For better comparison, the extracted traces from Fig. 9 are shown in Fig. 10. Fig. 10 shows that the traces extracted from Fig. 9(b) (red dashed line) are closer to the traces extracted from Fig. 9(c) (pink dashed line) than the traces extracted from Fig. 9(a) (black solid line). From the above results, one can conclude that the newly derived pure-viscoacoustic TTI wave equation can achieve more accurate numerical modeling results than that of the wave equation derived by Mu et al. (2022b) in complex attenuating anisotropic media.

#### 4.4. A modified BP 2007 model

To demonstrate the stability of our pure-viscoacoustic TTI wave equation in complex model, the modified BP 2007 model is employed to perform the wavefield simulation. The model is discretized by  $701 \times 451$  grid points with a uniform vertical and horizontal space step of 15 m, the model parameter as displayed in Fig. 11. A Ricker wavelet with the dominant frequency of 20 Hz is located at (5257.5 m, 10 m); the time step is 0.001 s; the reference frequency is 20 Hz. The ranks of the low-rank decomposition method are  $N_1 = 2$  and  $N_2 = 3$ . Fig. 12(a)–(b) shows the wavefields simulated by the coupled pseudo-viscoacoustic TTI wave equation of Qiao et al. (2020) at 1.5 and 2.5 s, respectively. Fig. 13(a)–(d) shows the wavefields generated by our pure-viscoacoustic TTI wave equation at 1.5, 2.5, 3.0 and 3.5 s, respectively. It can be distinctly seen that Fig. 12(a) produces the numerical instability (as pointed

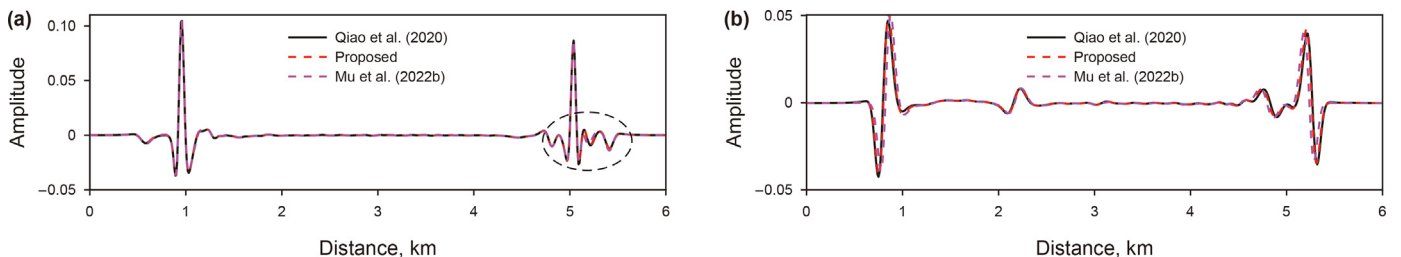


Fig. 10. Comparisons of the single-traces at the depth of  $z = 0.75$  km (a) and  $z = 1.55$  km (b). The black solid lines, the red dashed lines, and the pink dashed lines denote the traces extracted from Fig. 9(a), 9(b), and 9(c), respectively.

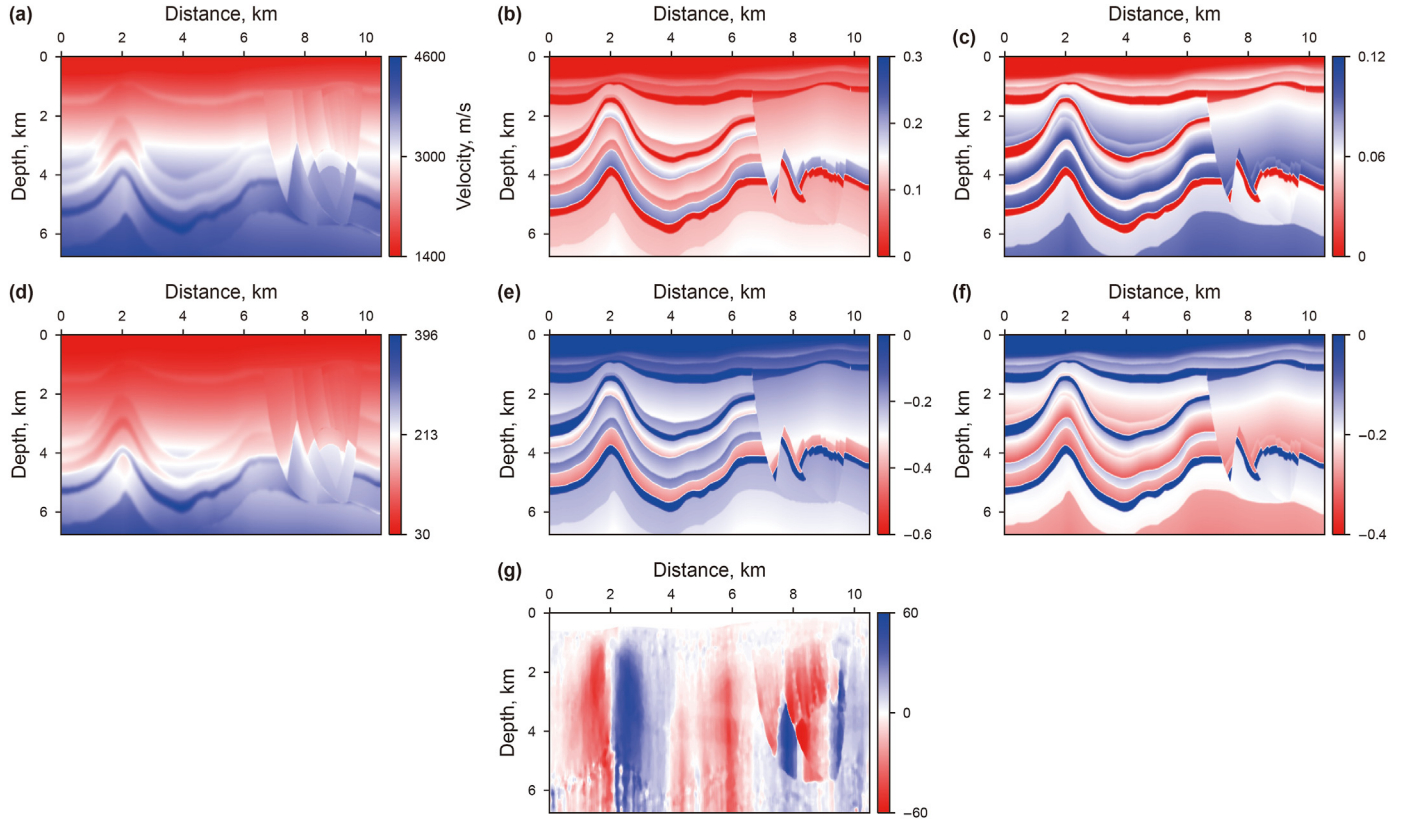


Fig. 11. BP 2007 model of velocity (a), Thomsen anisotropic parameters  $\epsilon$  (b) and  $\delta$  (c),  $Q_p$  (d),  $Q$ -related Thomsen anisotropic parameters  $\epsilon_Q$  (e) and  $\delta_Q$  (f), tilted parameter  $\varphi$  (g).

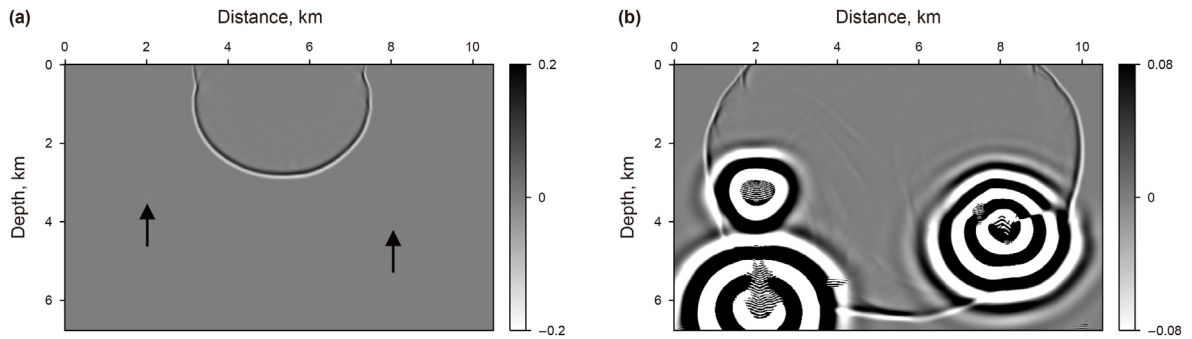


Fig. 12. Wavefield snapshots simulated by the coupled pseudo-viscoacoustic TTI wave equation proposed by Qiao et al. (2020) at  $t = 1.5$  s (a),  $t = 2.5$  s (b).

out by the black arrows), and the strong numerical instability is appeared in Fig. 12(b). On the contrast, the wavefields generated by our pure-viscoacoustic TTI wave equation can remain stable, as displayed in Fig. 13. The above results demonstrate that our pure-viscoacoustic TTI wave equation can obtain a more stable wavefield in complex media in comparison to the coupled pseudo-viscoacoustic TTI wave equations.

### 5. Discussion

In this paper, a new pure-viscoacoustic anisotropic wave equation is derived from the exact complex-valued dispersion relation in viscoelastic VTI media and we develop the HFDLRD method to accurately solve the proposed wave equation. The newly derived equation has higher accuracy than the previous wave equations, while also has drawback that requires huge computational resources. This is because the existence of the operator  $S_t$  in Eq. (24). To improve the computational efficiency, we provide a simplified

wave equation as follows:

We rewrite Eq. (11) as

$$V_p^2(\theta) = M_{11} \sin^2 \theta + M_{33} \cos^2 \theta + \frac{[M_{13}^2/M_{33} - M_{11}] \sin^2 \theta \cos^2 \theta}{(1 + \epsilon) + (\epsilon(2 \sin^2 \theta - 1) - 0.5(\epsilon - \delta) \sin^2 2\theta)}, \quad (32)$$

given that  $0.5(\epsilon - \delta) \sin^2 2\theta \leq 0.075$  for  $\epsilon \in (0, 0.4)$ ,  $\theta \in (0, 2\pi)$  and  $\delta \in (-0.2, 0.4)$ , we can make an assumption that  $0.5(\epsilon - \delta) \sin^2 2\theta \approx 0$ . In addition, we make an assumption that  $\sin^2 \theta \approx 0.5$ , because the average of  $\sin^2 \theta$  is 0.5 for  $\theta \in (0, 2\pi)$  (Huang et al., 2023). Therefore, Eq. (32) can be approximated as follows:

$$V_p^2(\theta) = M_{11} \sin^2 \theta + M_{33} \cos^2 \theta + \frac{[M_{13}^2/M_{33} - M_{11}] \sin^2 \theta \cos^2 \theta}{1 + \epsilon}. \quad (33)$$

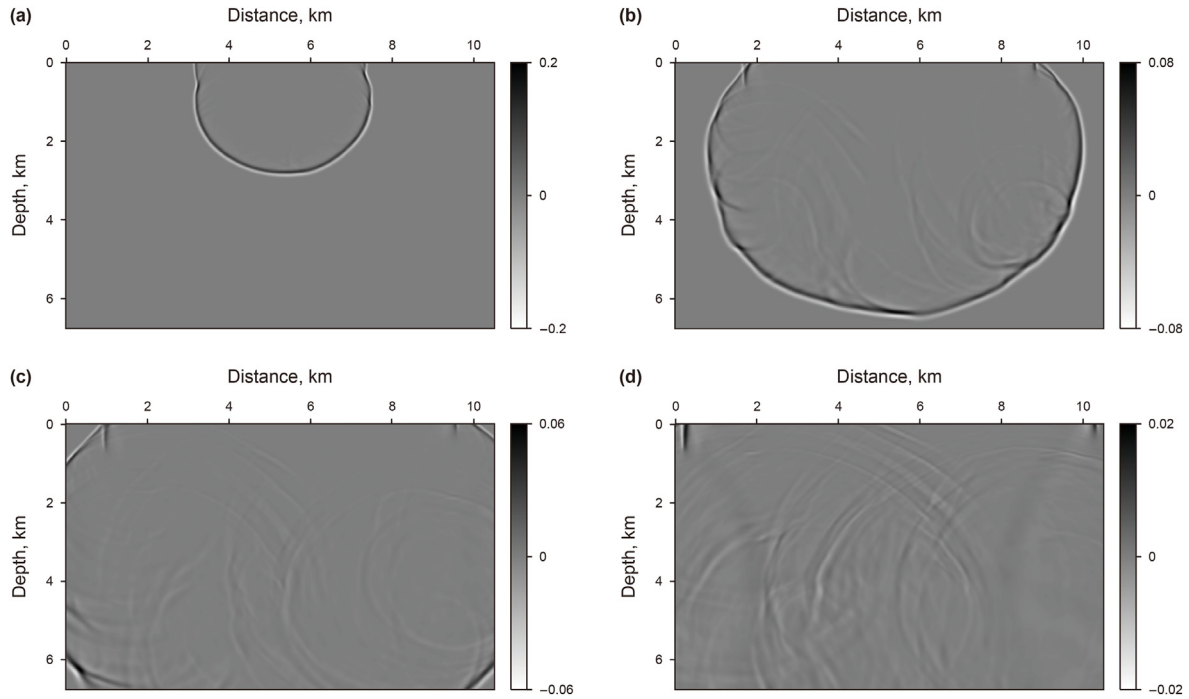


Fig. 13. Wavefield snapshots simulated by our pure-viscoacoustic TTI wave equation at  $t = 1.5$  s (a),  $t = 2.5$  s (b),  $t = 3.0$  s (c),  $t = 3.5$  s (d).

Using Eqs. (13) and (15), Eq. (33) can be formulated as

$$\omega^2 = \left( \eta_{11} k^{2\gamma_{11}} + \tau_{11}(i\omega) k^{2\gamma_{11}-1} \right) k_x^2 + \left( \eta_{33} k^{2\gamma_{33}} + \tau_{33}(i\omega) k^{2\gamma_{33}-1} \right) k_z^2 + \frac{\left[ \left( a_3 k^{2\lambda_{13}} + b_3(i\omega) k^{2\lambda_{13}-1} \right) - \left( \eta_{11} k^{2\gamma_{11}} + \tau_{11}(i\omega) k^{2\gamma_{11}-1} \right) \right] k_x^2 k_z^2}{1 + \varepsilon}. \tag{34}$$

Eq. (34) is the approximate dispersion relation of P-wave in VTI media. Based on Eq. (34), finally, the simplified time-space domain pure-viscoacoustic TTI wave equation is given as

To demonstrate the accuracy of the simplified pure-viscoacoustic TTI wave equation (Eq. (35)), we generate the wavefield snapshots at 0.5 s using the different wave equations. The model parameters are the same as those in Fig. 3(a). The Ricker wavelet with peak frequency of 25 Hz is located at the central of the model, the time step is 0.001 s, the reference frequency is 25 Hz.

$$\frac{\partial^2 p}{\partial t^2} = \left( \eta_{11} (-\nabla^2)^{\gamma_{11}} + \tau_{11} \frac{\partial}{\partial t} (-\nabla^2)^{\gamma_{11}-0.5} \right) \left( \cos^2 \varphi \frac{\partial^2}{\partial x^2} + \sin^2 \varphi \frac{\partial^2}{\partial z^2} - \sin(2\varphi) \frac{\partial^2}{\partial x \partial z} \right) p + \left( \eta_{33} (-\nabla^2)^{\gamma_{33}} + \tau_{33} \frac{\partial}{\partial t} (-\nabla^2)^{\gamma_{33}-0.5} \right) \left( \sin^2 \varphi \frac{\partial^2}{\partial x^2} + \cos^2 \varphi \frac{\partial^2}{\partial z^2} + \sin(2\varphi) k_x k_z \right) p + \frac{\left( a_3 (-\nabla^2)^{\lambda_{13}} + b_3 \frac{\partial}{\partial t} (-\nabla^2)^{\lambda_{13}-0.5} \right) \left( \cos^2 \varphi \sin^2 \varphi \left( \frac{\partial^4}{\partial x^4} + \frac{\partial^4}{\partial z^4} \right) + \left( \cos^4 \varphi + \sin^4 \varphi - \sin^2(2\varphi) \right) \frac{\partial^4}{\partial x^2 \partial z^2} \right) \left( -\eta_{11} (-\nabla^2)^{\gamma_{11}} - \tau_{11} \frac{\partial}{\partial t} (-\nabla^2)^{\gamma_{11}-0.5} \right) \left( +\cos(2\varphi) \sin(2\varphi) \frac{\partial^4}{\partial x^3 \partial z} - \cos(2\varphi) \sin(2\varphi) \frac{\partial^4}{\partial x \partial z^3} \right) p}{(1 + \varepsilon) \left( \frac{\partial^2}{\partial x^2} + \frac{\partial^2}{\partial z^2} \right)} + f. \tag{35}$$

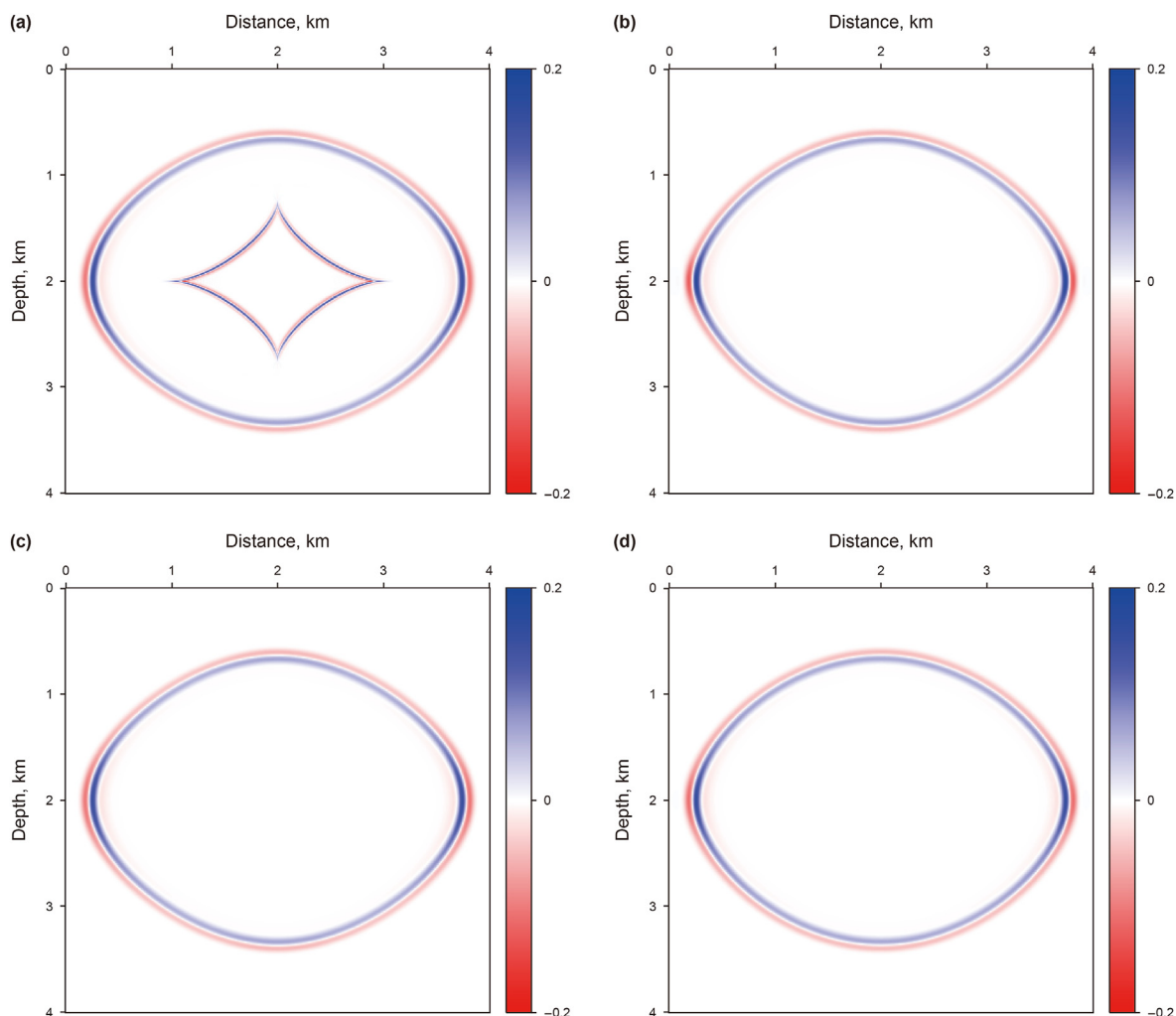


**Fig. 14.** Wavefield snapshots at 0.5 s generated by different wave equation. (a) The coupled pseudo-viscoacoustic TTI wave equation derived by Qiao et al. (2020). (b) The pure-viscoacoustic TTI wave equation proposed by Mu et al. (2022b). (c) The proposed pure-viscoacoustic TTI wave equation (Eq. (24)). (d) The proposed simplified pure-viscoacoustic TTI wave equation (Eq. (35)).

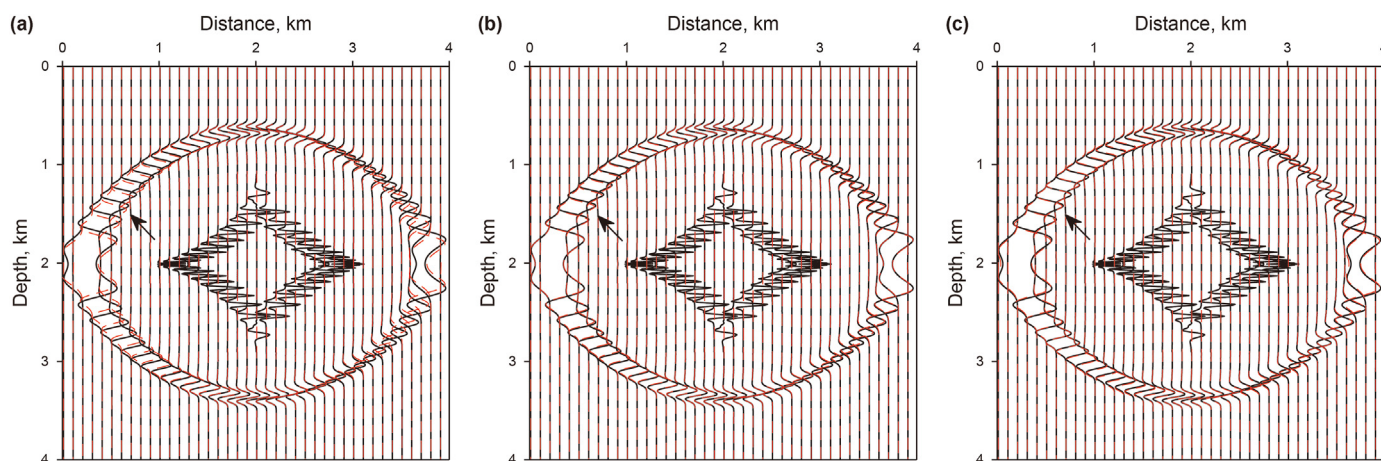


**Fig. 15.** Comparisons of wavefield snapshots from Fig. 14(a)–(d) in wiggle forms. (a) The wavefields generated by the pure-viscoacoustic TTI wave equation derived by Mu et al. (2022b) (Fig. 14(b)) (red dashed lines) and the reference wavefield (black solid lines). (b) The wavefields generated by the proposed pure-viscoacoustic TTI wave equation (Fig. 14(c)) (red dashed lines) and the reference wavefield (black solid lines). (c) The wavefields generated by the proposed simplified pure-viscoacoustic TTI wave equation (Fig. 14(d)) (red dashed lines) and the reference wavefield (black solid lines).

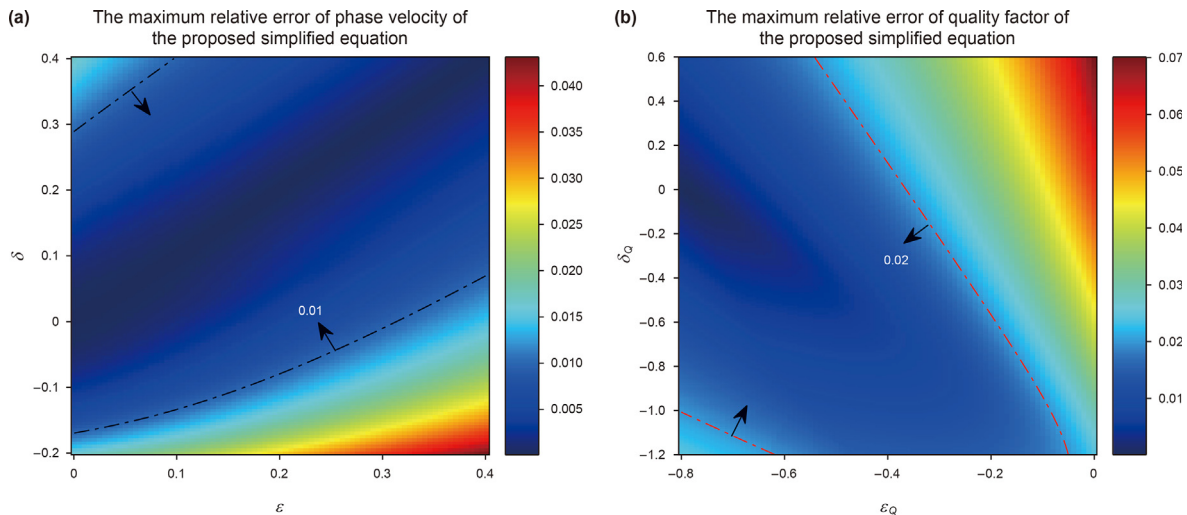


**Fig. 16.** The maximum relative error of the phase velocity and quality factor of the proposed simplified wave equation (Eq. (35)). (a) The maximum relative error of the phase velocity; (b) The maximum relative error of the quality factor. The model parameters are the same as those in Fig. 2.

Fig. 14 shows the wavefield snapshots at 0.5 s generated by the different wave equations. The ranks of the low-rank decomposition method are  $N_1 = 1$  and  $N_2 = 1$ . Fig. 15 are the comparisons of wavefield snapshots in a wiggle form. As pointed out by the black arrows in Fig. 15, one can notice that the wavefield snapshots generated by the proposed wave equation (Fig. 15(b)) and the proposed simplified wave equation (Fig. 15(c)) are in better match with the reference wavefield, in comparison with the previous wave equation (Fig. 15(a)). This result suggests that both the proposed wave equation and the proposed simplified wave equation can accurately simulate the kinematic characteristic of P-wave in attenuating anisotropic media. Additionally, compared to the proposed wave Eq. (24), the proposed simplified wave Eq. (35) requires less computational cost because it has concise expression. However, it also should be noted that the proposed simplified wave equation has made more approximation than the proposed wave equation (Eq. (24)) in the derivation of the wave equation. This leads to the fact that the accuracy of the proposed simplified wave equation is lower than the proposed wave equation. To further fairly evaluate the accuracy of the proposed simplified wave equation, we provide the maximum relative error of the phase velocity and quality factor of the proposed simplified wave equation, as shown in Fig. 16. By comparing Fig. 16 with Fig. 2, we can observe that the accuracy of the proposed simplified wave equation is higher than the previous wave equations, while it is lower than the proposed wave equation (Eq. (24)). As a result, from the above analysis, we can see that the two types of proposed pure-viscoacoustic anisotropic equations (i.e., Eqs. (24) and (35)) have their features, and we can choose between them based on our requirements.

Second, the numerical stability of wavefield simulation in attenuating anisotropic media also has attracted a lot of interesting (Mu et al., 2022b). We notice that although the pure-viscoacoustic TTI wave equation is more stable than the coupled pseudo-viscoacoustic TTI wave equation, numerical instability still occurs when simulating in some regions with rapidly changing tilt angle (Duvencek and Bakker, 2011; Yan and Liu, 2016). This numerical instability can be attributed to the fact that the acoustic approximation is used and all spatial derivatives in the direction of the anisotropic symmetry axis are neglected in the derivation of the wave equation (Duvencek and Bakker, 2011; Mu et al., 2022b). To

solve this problem, several measures (e.g., low-pass filter) can be used to address the instability to stabilize the computation results when simulating in complex media with a sharp tilt angle (Mu et al., 2020). Nevertheless, the kinematic and dynamic accuracy of the wavefield may be affected by these approaches to some extent. Therefore, the development of an accurate and suitable method to address these instabilities is our future work.

## 6. Conclusion

Based on the exact complex-valued dispersion relation in viscoelastic VTI media, we derive a new pure-viscoacoustic TTI wave equation in media with velocity anisotropy and attenuation anisotropy. This equation contains decoupled phase dispersion and amplitude dissipation terms, which makes it convenient to realize  $Q$ -compensated RTM. Theoretical analysis and numerical experiments demonstrate that our pure-viscoacoustic TTI wave equation has higher accuracy than the previous pure-viscoacoustic TTI wave equations in modeling seismic wave propagation in attenuating anisotropic media. For numerical simulation, we develop the HFDRD method to solve the proposed pure-viscoacoustic TTI wave equation. Numerical test of the simple two-layer shows that the HFDRD method can accurately calculate the seismic wave propagation in attenuating anisotropic media with strong attenuation. The newly derived pure-viscoacoustic TTI wave equation and the proposed numerical simulation method can be used as forward engines for viscoacoustic anisotropic RTM and FWI in attenuating anisotropic media.

## Declaration of competing interest

All authors certify that they have no affiliations with or involvement in any organization or entity with any financial interest or non-financial interest in the subject matter or materials discussed in this manuscript.

## Acknowledgements

We thank the editors and two anonymous reviewers for their insightful comments that significantly improved the quality of this paper. This study is supported by the Marine S&T Fund of Shandong

Province for Pilot National Laboratory for Marine Science and Technology (Qingdao) (No. 2021QNLM020001), the Major Scientific and Technological Projects of Shandong Energy Group (No. SNKJ2022A06-R23), the Funds of Creative Research Groups of China (No. 41821002), National Natural Science Foundation of China Outstanding Youth Science Fund Project (Overseas) (No. ZX20230152).

**Appendix A**

The exact and approximate TTI complex-valued P-wave phase velocity formulas

Starting from Eq. (3), we rotate the symmetry axis and the exact complex-valued phase velocity formula for P-wave in the viscoelastic TTI media can be written as

$$V_p(\theta, \varphi) = \left[ \frac{1}{2\rho} \left( M_{11} \sin^2(\varphi - \theta) + M_{33} \cos^2(\varphi - \theta) + M_{55} + E \right) \right]^{1/2},$$

$$E = \sqrt{\frac{\left( (M_{33} - M_{55}) \cos^2(\varphi - \theta) + (M_{55} - M_{11}) \sin^2(\varphi - \theta) \right)^2 + 4(M_{13} - M_{55})^2 \sin^2(\varphi - \theta) \cos^2(\varphi - \theta)}{}}.$$

(A-1)

Similarly, the proposed approximate complex-valued phase velocity formula in TTI media can be expressed as

$$V_p^2(\theta, \varphi) = M_{11} \sin^2(\varphi - \theta) + M_{33} \cos^2(\varphi - \theta) + \frac{\left[ \frac{M_{13}^2}{M_{33} - M_{11}} \right] \sin^2(\varphi - \theta) \cos^2(\varphi - \theta)}{\left[ (1 + 2\varepsilon) \sin^2(\varphi - \theta) + \cos^2(\varphi - \theta) - 2(\varepsilon - \delta) \sin^2(\varphi - \theta) \cos^2(\varphi - \theta) \right]}.$$

(A-2)

---


$$\frac{\partial^2 \sigma_{xx}}{\partial t^2} = \left( \eta_{11} (-\nabla^2)^{\gamma_{11}} + \tau_{11} \frac{\partial}{\partial t} (-\nabla^2)^{\gamma_{11}/2-0.5} \right) \left( \cos^2 \varphi \frac{\partial^2}{\partial x^2} + \sin^2 \varphi \frac{\partial^2}{\partial z^2} - \sin 2\varphi \frac{\partial^2}{\partial x \partial z} \right) \sigma_{xx}$$

$$+ \left( \eta_{13} (-\nabla^2)^{\gamma_{13}} + \tau_{13} \frac{\partial}{\partial t} (-\nabla^2)^{\gamma_{13}/2-0.5} \right) \left( \sin^2 \varphi \frac{\partial^2}{\partial x^2} + \cos^2 \varphi \frac{\partial^2}{\partial z^2} + \sin 2\varphi \frac{\partial^2}{\partial x \partial z} \right) \sigma_{zz} + f_x,$$

(B-1)

$$\frac{\partial^2 \sigma_{zz}}{\partial t^2} = \left( \eta_{13} (-\nabla^2)^{\gamma_{13}} + \tau_{13} \frac{\partial}{\partial t} (-\nabla^2)^{\gamma_{13}/2-0.5} \right) \left( \cos^2 \varphi \frac{\partial^2}{\partial x^2} + \sin^2 \varphi \frac{\partial^2}{\partial z^2} - \sin 2\varphi \frac{\partial^2}{\partial x \partial z} \right) \sigma_{xx}$$

$$+ \left( \eta_{33} (-\nabla^2)^{\gamma_{33}} + \tau_{33} \frac{\partial}{\partial t} (-\nabla^2)^{\gamma_{33}/2-0.5} \right) \left( \sin^2 \varphi \frac{\partial^2}{\partial x^2} + \cos^2 \varphi \frac{\partial^2}{\partial z^2} + \sin 2\varphi \frac{\partial^2}{\partial x \partial z} \right) \sigma_{zz} + f_z,$$

(B-2)

---

According to Eq. (36), Qiao et al. (2020) also give the expressions of the directionally dependent phase velocity, quality factor and attenuation coefficient of P-wave, which can be written as follows:

$$\hat{v}_p(\theta) = \left( \text{Re} \left( \frac{1}{V_p} \right) \right)^{-1},$$

(A-3)

$$\hat{Q}_p(\theta) = \frac{\text{Re} \left( V_p^2 \right)}{\text{Im} \left( V_p^2 \right)},$$

(A-4)

$$\hat{\alpha}_p(\theta) = -\omega \text{Im} \left( \frac{1}{V_p} \right).$$

(A-5)

**Appendix B**

The HFDLRD method for solving the coupled pseudo-viscoacoustic TTI wave equation

Qiao et al. (2020) proposed a coupled pseudo-viscoacoustic TTI wave equation, which can be rewritten as

where  $\sigma_{xx}$  and  $\sigma_{zz}$  denote the horizontal component and vertical component of stress, respectively.  $f_x$  and  $f_z$  represent the horizontal component and vertical component of source function, respectively. According to the HFDRD method illustrated previously, Eqs. (B-1) and (B-2) can be reformulated as

$$\begin{aligned} \frac{\partial^2 \sigma_{xx}}{\partial t^2} = & \left( \eta_{11} \mathcal{F}^{-1} \left( k^{2\gamma_{11}} \mathcal{F}(\sigma_{xx}) \right) + \tau_{11} \mathcal{F}^{-1} \left( k^{2\gamma_{11}-1} \mathcal{F} \left( \frac{\partial \sigma_{xx}}{\partial t} \right) \right) \right) \left( \cos^2 \varphi \frac{\partial^2}{\partial x^2} + \sin^2 \varphi \frac{\partial^2}{\partial z^2} - \sin 2\varphi \frac{\partial^2}{\partial x \partial z} \right) \\ & + \left( \eta_{13} \mathcal{F}^{-1} \left( k^{2\gamma_{13}} \mathcal{F}(\sigma_{zz}) \right) + \tau_{13} \mathcal{F}^{-1} \left( k^{2\gamma_{13}-1} \mathcal{F} \left( \frac{\partial \sigma_{zz}}{\partial t} \right) \right) \right) \left( \sin^2 \varphi \frac{\partial^2}{\partial x^2} + \cos^2 \varphi \frac{\partial^2}{\partial z^2} + \sin 2\varphi \frac{\partial^2}{\partial x \partial z} \right) + f_x, \end{aligned} \quad (\text{B-3})$$

$$\begin{aligned} \frac{\partial^2 \sigma_{zz}}{\partial t^2} = & \left( \eta_{13} \mathcal{F}^{-1} \left( k^{2\gamma_{13}} \mathcal{F}(\sigma_{xx}) \right) + \tau_{13} \mathcal{F}^{-1} \left( k^{2\gamma_{13}-1} \mathcal{F} \left( \frac{\partial \sigma_{xx}}{\partial t} \right) \right) \right) \left( \cos^2 \varphi \frac{\partial^2}{\partial x^2} + \sin^2 \varphi \frac{\partial^2}{\partial z^2} - \sin 2\varphi \frac{\partial^2}{\partial x \partial z} \right) \\ & + \left( \eta_{33} \mathcal{F}^{-1} \left( k^{2\gamma_{33}} \mathcal{F}(\sigma_{zz}) \right) + \tau_{33} \mathcal{F}^{-1} \left( k^{2\gamma_{33}-1} \mathcal{F} \left( \frac{\partial \sigma_{zz}}{\partial t} \right) \right) \right) \left( \sin^2 \varphi \frac{\partial^2}{\partial x^2} + \cos^2 \varphi \frac{\partial^2}{\partial z^2} + \sin 2\varphi \frac{\partial^2}{\partial x \partial z} \right) + f_z. \end{aligned} \quad (\text{B-4})$$

Finally, based on Eq. (31) and the finite-difference method, Eqs. (B-3) and (B-4) can be conveniently solved by the HFDRD method.

## References

- Aki, K., Richards, P., 1980. *Quantitative Seismology: Theory and Methods*. Freeman, San Francisco, CA. <https://doi.org/10.1121/1.385057>.
- Alkhalifah, T., 2000. An acoustic wave equation for anisotropic media. *Geophysics* 65 (4), 1239–1250. <https://doi.org/10.1190/1.1444815>.
- Bai, T., Tsvankin, I., 2016. Time-domain finite-difference modeling for attenuative anisotropic media. *Geophysics* 81 (2), C69–C77. <https://doi.org/10.1190/geo2015-0424.1>.
- Behura, J., Tsvankin, I., 2009. Estimation of interval anisotropic attenuation from reflection data. *Geophysics* 74 (6), A69–A74. <https://doi.org/10.1190/1.3191733>.
- Best, A.L., Sothcott, J., McCann, C., 2007. A laboratory study of seismic velocity and attenuation anisotropy in near-surface sedimentary rocks. *Geophys. Prospect.* 55 (5), 609–625. <https://doi.org/10.1111/j.1365-2478.2007.00642.x>.
- Carcione, J.M., 1992. Anisotropic Q and velocity dispersion of finely layered media. *Geophys. Prospect.* 40 (7), 761–783. <https://doi.org/10.1111/j.1365-2478.1992.tb00551.x>.
- Carcione, J.M., 2010. A generalization of the Fourier pseudo-spectral method. *Geophysics* 75 (6), A53–A56. <https://doi.org/10.1190/1.3509472>.
- Carcione, J.M., Cavallini, F., Mainardi, F., et al., 2002. Time-domain seismic modeling of constant Q wave propagation using fractional derivatives. *Pure Appl. Geophys.* 159 (7), 1719–1736. <https://doi.org/10.1007/s00024-002-8705-z>.
- Carcione, J.M., Kosloff, D., Kosloff, R., 1988. Wave propagation simulation in a linear viscoacoustic medium. *Geophys. J. Int.* 93 (2), 393–401. <https://doi.org/10.1111/j.1365-246X.1988.tb02010.x>.
- Carcione, J.M., Picotti, S., Santos, J.E., 2012. Numerical experiments of fracture-induced velocity and attenuation anisotropy. *Geophys. J. Int.* 191 (3), 1179–1191. <https://doi.org/10.1111/j.1365-246X.2012.05697.x>.
- Cerjan, C., Kosloff, D., Kosloff, R., et al., 1985. A nonreflecting boundary condition for discrete acoustic and elastic wave equations. *Geophysics* 50 (4), 705–708. <https://doi.org/10.1190/1.1441945>.
- Chen, H., Zhou, H., Li, Q., Wang, Y., 2016. Two efficient modeling schemes for fractional Laplacian viscoacoustic wave equation. *Geophysics* 81 (5), T233–T249. <https://doi.org/10.1190/geo2015-0660.1>.
- Chen, H., Zhou, H., Jiang, S., et al., 2019a. Fractional Laplacian viscoacoustic wave equation low-rank temporal extrapolation. *IEEE Access* 7, 93187–93197. <https://doi.org/10.1109/ACCESS.2019.2927760>.
- Chen, H., Zhou, H., Rao, Y., et al., 2019b. A matrix-transform numerical solver for fractional Laplacian viscoacoustic wave equation. *Geophysics* 84 (4), T283–T297. <https://doi.org/10.1190/geo2018-0271.1>.
- Chichinina, T., Obolentseva, I., Gik, L., et al., 2009. Attenuation anisotropy in the linear-slip model: interpretation of physical modeling data. *Geophysics* 74 (5), WB165–WB176. <https://doi.org/10.1190/1.3173806>.
- Chu, C., Macy, B.K., Anno, P.D., 2011. Approximation of pure acoustic seismic wave propagation in TTI media. *Geophysics* 76 (5), WB97–WB107. <https://doi.org/10.1190/geo2011-0092.1>.
- Da Silva, N.V., Yao, G., Warner, M., 2019. Wave modeling in viscoacoustic media with transverse isotropy. *Geophysics* 84 (1), C41–C56. <https://doi.org/10.1190/geo2017-0695.1>.

- Deng, F., McMechan, G.A., 2007. True-amplitude prestack depth migration. *Geophysics* 72 (3), S155–S166. <https://doi.org/10.1190/1.2714334>.
- Du, X., Bancroft, J.C., Lines, L.R., 2007. Anisotropic reverse-time migration for tilted TI media. *Geophys. Prospect.* 55 (6), 853–869. <https://doi.org/10.1111/j.1365-2478.2007.00652.x>.
- Dutta, G., Schuster, G.T., 2014. Attenuation compensation for least squares reverse time migration using the viscoacoustic-wave equation. *Geophysics* 79 (6), S251–S262. <https://doi.org/10.1190/geo2013-0414.1>.
- Duveneck, E., Bakker, P.M., 2011. Stable P-wave modeling for reverse time migration in tilted TI media. *Geophysics* 76 (2), S65–S75. <https://doi.org/10.1190/1.3533964>.
- Duveneck, E., Milcic, P., Bakker, P.M., et al., 2008. Acoustic VTI wave equations and their application for anisotropic reverse-time migration. In: 78th Annual International Meeting, SEG Expanded Abstracts, pp. 2186–2190. <https://doi.org/10.1190/1.3059320>.
- Emmerich, H., Korn, M., 1987. Incorporation of attenuation into time domain computations of seismic wave fields. *Geophysics* 52 (2), 1252–1264. <https://doi.org/10.1190/1.1442386>.
- Fathalian, A., Trad, D.O., Innanen, K.A., 2021. Q-compensated reverse time migration in tilted transversely isotropic media. *Geophysics* 86 (1), S73–S89. <https://doi.org/10.1190/geo2019-0466.1>.
- Fletcher, R., Du, X., Fowler, P., 2009. Reverse-time migration in tilted transversely isotropic (TTI) media. *Geophysics* 74 (6), WCA179–WCA187. <https://doi.org/10.1190/1.3269902>.
- Fomel, S., 2004. On anelliptic approximations for qP velocities in VTI media. *Geophys. Prospect.* 52 (3), 247–259. <https://doi.org/10.1111/j.1365-2478.2004.00413.x>.
- Fomel, S., Ying, L., Song, X., 2013. Seismic wave extrapolation using lowrank symbol approximation. *Geophys. Prospect.* 61 (3), 526–536. <https://doi.org/10.1111/j.1365-2478.2012.01064.x>.
- Guo, P., McMechan, G.A., 2017. Sensitivity of 3D 3C synthetic seismograms to anisotropic attenuation and velocity in reservoir models. *Geophysics* 82 (2), T79–T95. <https://doi.org/10.1190/geo2016-0321.1>.
- Guo, P., McMechan, G.A., Guan, H., 2016. Comparison of two viscoacoustic propagators for Q-compensated reverse time migration. *Geophysics* 81 (5), S281–S297. <https://doi.org/10.1190/geo2015-0557.1>.
- Hao, Q., Alkhalifah, T., 2017. An acoustic eikonal equation for attenuating VTI media. *Geophysics* 82 (1). <https://doi.org/10.1190/segam2016-13857107.1>. C9–C20.
- Hao, Q., Alkhalifah, T., 2019. Viscoacoustic anisotropic wave equations. *Geophysics* 84 (6), C323–C337. <https://doi.org/10.1190/geo2018-0865.1>.
- Huang, J., Mao, Q., Mu, X., et al., 2023. Least-squares reverse time migration based on an efficient pure qP-wave equation. *Geophys. Prospect.* 00, 1–22. <https://doi.org/10.1111/1365-2478.13326>.
- Kjartansson, E., 1979. Constant-Q wave propagation and attenuation. *J. Geophys. Res.* 84 (B9), 4737–4748. <https://doi.org/10.1029/JB084iB09p04737>.
- Li, B., Stovas, A., 2021. Decoupled approximation and separate extrapolation of P- and SV-waves in transversely isotropic media. *Geophysics* 86 (4), C133–C142. <https://doi.org/10.1190/geo2020-0232.1>.
- Li, Q., Zhou, H., Zhang, Q., et al., 2016. Efficient reverse time migration based on fractional Laplacian viscoacoustic wave equation. *Geophys. J. Int.* 204 (1), 488–504. <https://doi.org/10.1093/gji/ggv456>.
- Liang, K., Cao, D., Sun, S., et al., 2023. Decoupled wave equation and forward modeling of qP wave in VTI media with the new acoustic approximation. *Geophysics* 88 (1), WA335–WA344. <https://doi.org/10.1190/geo2022-0292.1>.

- Liu, E., Crampin, S., Varela, I., et al., 2007. Velocity and attenuation anisotropy: implication of seismic fracture characterizations. *Lead. Edge* 26 (9), 1170–1174. <https://doi.org/10.1190/1.2780788>.
- Liu, H., Luo, Y., 2021. An analytic signal-based accurate time-domain viscoacoustic wave equation from the constant Q theory. *Geophysics* 86 (3), T117–T126. <https://doi.org/10.1190/geo2020-0154.1>.
- Lynn, H.B., Campagna, D., Simon, K.M., et al., 1999. Relationship of P-wave seismic attributes, azimuthal anisotropy, and commercial gas pay in 3-D P-wave multiazimuth data, Rulison Field, Piceance Basin, Colorado. *Geophysics* 64 (4), 1293–1311. <https://doi.org/10.1190/1.1444635>.
- McDonal, F.J., Angona, F.A., Mills, R.L., et al., 1958. Attenuation of shear and compressional waves in Pierre shale. *Geophysics* 23 (3), 421–439. <https://doi.org/10.1190/1.1438489>.
- Mu, X., Huang, J., Li, Z., et al., 2022a. Attenuation compensation and anisotropy correction in reverse time migration for attenuating tilted transversely isotropic media. *Surv. Geophys.* 43 (3), 737–773. <https://doi.org/10.1007/s10712-022-09707-2>.
- Mu, X., Huang, J., Yang, J., et al., 2022b. Modeling of Pure visco-qP-wave propagation in attenuating tilted transversely isotropic (TTI) media based on decoupled fractional Laplacians. *Geophysics* 87 (4), T291–T313. <https://doi.org/10.1190/geo2021-0440.1>.
- Mu, X., Huang, J., Wen, L., et al., 2021. Modeling viscoacoustic wave propagation using a new spatial variable-order fractional Laplacian wave equation. *Geophysics* 86 (6), T487–T507. <https://doi.org/10.1190/geo2020-0610.1>.
- Mu, X., Huang, J., Yong, P., et al., 2020. Modeling of pure qP- and qSV-waves in tilted transversely isotropic media with the optimal quadratic approximation. *Geophysics* 85 (2), C71–C89. <https://doi.org/10.1190/geo2018-0460.1>.
- Qiao, Z., Chen, T., Sun, C., 2022. Anisotropic attenuation compensated reverse time migration of pure qP-wave in transversely isotropic attenuating media. *Surv. Geophys.* 43 (5), 1435–1467. <https://doi.org/10.1007/s10712-022-09717-0>.
- Qiao, Z., Sun, C., Tang, J., 2020. Modelling of viscoacoustic wave propagation in transversely isotropic media using decoupled fractional Laplacians. *Geophys. Prospect.* 68 (8), 2400–2418. <https://doi.org/10.1111/1365-2478.13006>.
- Qiao, Z., Sun, C., Wu, D., 2019. Theory and modelling of constant-Q viscoelastic anisotropic media using fractional derivative. *Geophys. J. Int.* 217 (2), 798–815. <https://doi.org/10.1093/gji/ggz050>.
- Qu, Y., Huang, J., Li, Z., et al., 2017. Attenuation compensation in anisotropic least-squares reverse time migration. *Geophysics* 82 (6), S411–S423. <https://doi.org/10.1190/geo2016-0677.1>.
- Robertsson, J.O., Blanch, J.O., Symes, W.W., 1994. Viscoelastic finite difference modeling. *Geophysics* 59 (9), 1444–1456. <https://doi.org/10.1190/1.1443701>.
- Sun, J., Zhu, T., Fomel, S., 2015. Viscoacoustic modeling and imaging using low-rank approximation. *Geophysics* 80 (5), A103–A108. <https://doi.org/10.1190/geo2015-0083.1>.
- Sun, J., Fomel, S., Zhu, T., et al., 2016. Q-compensated least-squares reverse time migration using low-rank one-step wave extrapolation. *Geophysics* 81 (4), S271–S279. <https://doi.org/10.1190/geo2015-0520.1>.
- Thomsen, L., 1986. Weak elastic anisotropy. *Geophysics* 51 (10), 1954–1966. <https://doi.org/10.1190/1.1442051>.
- Tsvankin, I., 1996. P-wave signatures and notation for transversely isotropic media: An overview. *Geophysics* 61 (2), 467–483. <https://doi.org/10.1190/1.1443974>.
- Usher, P.J., Kendall, J.M., Kelly, C.M., et al., 2017. Measuring changes in fracture properties from temporal variations in anisotropic attenuation of microseismic waveforms. *Geophys. Prospect.* 65 (1), 347–362. <https://doi.org/10.1111/1365-2478.12551>.
- Wang, N., Xing, G., Zhu, T., et al., 2022. Propagating seismic waves in VTI attenuating media using fractional viscoelastic wave equation. *J. Geophys. Res.* 127 (4), e2021JB023280. <https://doi.org/10.1029/2021JB023280>.
- Wang, N., Zhou, H., Chen, H., et al., 2018. A constant fractional-order viscoelastic wave equation and its numerical simulation scheme. *Geophysics* 83 (1), T39–T48. <https://doi.org/10.1190/geo2016-0609.1>.
- Wang, N., Zhu, T., Zhou, H., et al., 2020. Fractional Laplacians viscoacoustic wavefield modeling with k-space-based time-stepping error compensating scheme. *Geophysics* 85 (1), T1–T13. <https://doi.org/10.1190/geo2019-0151.1>.
- Xu, S., Stovas, A., Alkhalifah, T., et al., 2020. New acoustic approximation for transversely isotropic media with a vertical symmetry axis. *Geophysics* 85 (1), C1–C12. <https://doi.org/10.1190/geo2019-0100.1>.
- Xu, W., Li, Z., Wang, J., et al., 2015. A Pure viscoacoustic equation for VTI media applied in anisotropic RTM. *J. Geophys. Eng.* 12 (6), 969–977. <https://doi.org/10.1088/1742-2132/12/6/969>.
- Yan, J., Liu, H., 2016. Modeling of pure acoustic wave in tilted transversely isotropic media using optimized pseudo-differential operators. *Geophysics* 81 (3), T91–T106. <https://doi.org/10.1190/geo2015-0111.1>.
- Yang, J., Zhu, H., 2018. A time-domain complex-valued wave equation for modelling visco-acoustic wave propagation. *Geophys. J. Int.* 215 (2), 1064–1079. <https://doi.org/10.1093/gji/ggy323>.
- Yao, J., Zhu, T., Hussain, F., et al., 2017. Locally solving fractional Laplacian viscoacoustic wave equation using Hermite distributed approximating functional method. *Geophysics* 82 (2), T59–T67. <https://doi.org/10.1190/geo2016-0269.1>.
- Zhan, G., Pestana, R., Stoffa, P., 2012. Decoupled equations for reverse time migration in tilted transversely isotropic media. *Geophysics* 77 (2), T37–T45. <https://doi.org/10.1190/geo2011-0175.1>.
- Zhang, Y., Chen, T., Liu, Y., et al., 2023. High-Temporal-accuracy viscoacoustic wave propagation based on k-space compensation and the fractional zener model. *Surv. Geophys.* 44 (3), 821–845. <https://doi.org/10.1007/s10712-022-09765-6>.
- Zhang, Y., Liu, Y., Xu, S., 2020a. Anisotropic viscoacoustic wave modelling in VTI media using frequency-dependent complex velocity. *J. Geophys. Eng.* 17 (4), 700–717. <https://doi.org/10.1093/jge/gxaa023>.
- Zhang, Y., Liu, Y., Xu, S., 2020b. Arbitrary-order Taylor series expansion based viscoacoustic wavefield simulation in 3D vertical transversely isotropic media. *Geophys. Prospect.* 68 (8), 2379–2399. <https://doi.org/10.1111/1365-2478.12999>.
- Zhang, Y., Zhang, H., Zhang, G., 2011. A stable TTI reverse time migration and its implementation. *Geophysics* 76 (3), WA3–WA11. <https://doi.org/10.1190/1.3554411>.
- Zhang, Z., Alkhalifah, T., Wu, Z., 2019. A hybrid finite-difference/low-rank solution to anisotropy acoustic wave equations. *Geophysics* 84 (2), T83–T91. <https://doi.org/10.1190/geo2018-0333.1>.
- Zhou, H., Liu, Y., Wang, J., 2022. Two exact first-order k-space formulations for low-rank viscoacoustic wave propagation on staggered grids. *Petrol. Sci.* 20 (3), 1521–1531. <https://doi.org/10.1016/j.petsci.2022.10.012>.
- Zhou, H., Zhang, G., Bloor, R., 2006. An anisotropic acoustic wave equation for modeling and migration in 2D TTI media. In: 76th Annual International Meeting. SEG, Expanded Abstracts, pp. 194–198. <https://doi.org/10.1190/1.2369913>.
- Zhu, T., 2017. Numerical simulation of seismic wave propagation in viscoelastic-anisotropic media using frequency-independent Q wave equation. *Geophysics* 82 (4), WA1–WA10. <https://doi.org/10.1190/geo2016-0635.1>.
- Zhu, T., Bai, T., 2019. Efficient modeling of wave propagation in a vertical-transversely isotropic attenuative medium based on fractional Laplacian. *Geophysics* 84 (3), T121–T131. <https://doi.org/10.1190/geo2018-0538.1>.
- Zhu, T., Carcione, J., Harris, J.M., 2013. Approximating constant-Q seismic propagation in the time domain. *Geophys. Prospect.* 61 (5), 931–940. <https://doi.org/10.1111/1365-2478.12044>.
- Zhu, T., Harris, J.M., 2014. Modeling acoustic wave propagation in heterogeneous attenuating media using decoupled fractional Laplacians. *Geophysics* 79 (3), T105–T116. <https://doi.org/10.1190/geo2013-0245.1>.
- Zhu, T., Harris, J.M., Biondi, B., 2014. Q-compensated reverse-time migration. *Geophysics* 79 (3), S77–S87. <https://doi.org/10.1190/geo2013-0344.1>.
- Zhu, Y., Tsvankin, I., 2006. Plane-wave propagation in attenuative transversely isotropic media. *Geophysics* 71 (2), T17–T30. <https://doi.org/10.1190/1.2187792>.
- Zhu, Y., Tsvankin, I., Vasconcelos, I., 2007. Effective attenuation anisotropy of thin-layered media. *Geophysics* 72 (5), D93–D106. <https://doi.org/10.1190/1.2754185>.
- Zhubayev, A., Houben, M.E., Smeulders, D.M., et al., 2016. Ultrasonic-velocity and attenuation anisotropy of shales, Whitby, United Kingdom. *Geophysics* 81 (1), D45–D56. <https://doi.org/10.1190/geo2015-0211.1>.